ARMY RESEARCH LABORATORY

A Continuum Description of Nonlinear Elasticity, Slip and Twinning, With Application to Sapphire

by J. D. Clayton

ARL-RP-246 **March 2009**

A reprint from the *Proceedings of the Royal Society A*, vol. 465, pp. 307–334, 2009.

NOTICES

Disclaimers

The findings in this report are not to be construed as an official Department of the Army position unless so designated by other authorized documents.

Citation of manufacturer's or trade names does not constitute an official endorsement or approval of the use thereof.

Destroy this report when it is no longer needed. Do not return it to the originator.

Army Research Laboratory

Aberdeen Proving Ground, MD 21005-5069

ARL-RP-246 **March 2009**

A Continuum Description of Nonlinear Elasticity, Slip and Twinning, With Application to Sapphire

J. D. Clayton

Weapons and Materials Research Directorate, ARL

A reprint from the *Proceedings of the Royal Society A*, vol. 465, pp. 307–334, 2009.

REPORT DOCUMENTATION PAGE

Form Approved
OMB No. 0704-0188

1. REPORT DATE *(DD-MM-YYYY)*	2. REPORT TYPE	3. DATES COVERED (From - To)
March 2009	Reprint	October 2007–October 2008

4. TITLE AND SUBTITLE
A Continuum Description of Nonlinear Elasticity, Slip and Twinning, With Application to Sapphire

5a. CONTRACT NUMBER

5b. GRANT NUMBER

5c. PROGRAM ELEMENT NUMBER

6. AUTHOR(S)
J. D. Clayton

5d. PROJECT NUMBER
AH80

5e. TASK NUMBER

5f. WORK UNIT NUMBER

7. PERFORMING ORGANIZATION NAME(S) AND ADDRESS(ES)
U.S. Army Research Laboratory
ATTN: AMSRD-ARL-WM-TD
Aberdeen Proving Ground, MD 21005-5069

8. PERFORMING ORGANIZATION REPORT NUMBER
ARL-RP-246

9. SPONSORING/MONITORING AGENCY NAME(S) AND ADDRESS(ES)

10. SPONSOR/MONITOR'S ACRONYM(S)

11. SPONSOR/MONITOR'S REPORT NUMBER(S)

12. DISTRIBUTION/AVAILABILITY STATEMENT
Approved for public release; distribution is unlimited.

13. SUPPLEMENTARY NOTES
A reprint from the *Proceedings of the Royal Society A*, vol. 465, pp. 307–334, 2009.

14. ABSTRACT

A model is developed for elasticity, plasticity and twinning in anisotropic single crystals subjected to large deformations. Dislocation glide and deformation twinning are dissipative, while energy storage mechanisms associated with dislocation lines and twin boundaries are described via scalar internal state variables. Concepts from continuum crystal plasticity are invoked, with shearing rates on discrete glide and twinning systems modelled explicitly. The model describes aspects of thermomechanical behaviour of single crystals of alumina over a range of loading conditions. Resolved shear stresses necessary for glide or twin nucleation at low to moderate temperatures are estimated from nonlinear elastic calculations, theoretical considerations of Peierls barriers and stacking fault energies and observations from shock physics experiments. These estimates are combined with the existing data from high-temperature experiments to provide initial yield conditions spanning a wide range of temperatures. The model reflects hardening of glide and twin systems from dislocations accumulated during basal slip. Residual elastic volume changes, predicted from nonlinear elastic considerations and approximated dislocation line energies, are positive and proportional to the dislocation line density. While the model suggests that generation of very large dislocation densities could influence the pressure–volume response, volume increases from defects are predicted to be small in crystals deformed via basal glide on a single system.

15. SUBJECT TERMS
ceramic, plasticity, defects, modeling, alumina, twinning

16. SECURITY CLASSIFICATION OF:			17. LIMITATION OF ABSTRACT	18. NUMBER OF PAGES	19a. NAME OF RESPONSIBLE PERSON
a. REPORT	b. ABSTRACT	c. THIS PAGE			John D. Clayton
Unclassified	Unclassified	Unclassified	UU	38	19b. TELEPHONE NUMBER (*Include area code*) 410-278-6146

PROCEEDINGS OF THE ROYAL SOCIETY A

Proc. R. Soc. A (2009) **465**, 307–334
doi:10.1098/rspa.2008.0281
Published online 21 October 2008

A continuum description of nonlinear elasticity, slip and twinning, with application to sapphire

By J. D. Clayton*

Impact Physics, U.S. Army Research Laboratory, Aberdeen Proving Ground, MD 21005-5066, USA

A model is developed for elasticity, plasticity and twinning in anisotropic single crystals subjected to large deformations. Dislocation glide and deformation twinning are dissipative, while energy storage mechanisms associated with dislocation lines and twin boundaries are described via scalar internal state variables. Concepts from continuum crystal plasticity are invoked, with shearing rates on discrete glide and twinning systems modelled explicitly. The model describes aspects of thermomechanical behaviour of single crystals of alumina over a range of loading conditions. Resolved shear stresses necessary for glide or twin nucleation at low to moderate temperatures are estimated from nonlinear elastic calculations, theoretical considerations of Peierls barriers and stacking fault energies and observations from shock physics experiments. These estimates are combined with the existing data from high-temperature experiments to provide initial yield conditions spanning a wide range of temperatures. The model reflects hardening of glide and twin systems from dislocations accumulated during basal slip. Residual elastic volume changes, predicted from nonlinear elastic considerations and approximated dislocation line energies, are positive and proportional to the dislocation line density. While the model suggests that generation of very large dislocation densities could influence the pressure–volume response, volume increases from defects are predicted to be small in crystals deformed via basal glide on a single system.

Keywords: crystal plasticity; twinning; alumina

1. Introduction

When subjected to large deformations or mechanical stresses, crystalline solids may deform by a number of mechanisms. In ductile crystals, where the dislocation mobility is sufficiently high in an adequate number of directions, dislocation glide is often the predominant accommodation mode for deviatoric deformations at stresses above the elastic limit. However, under different circumstances, inelastic strains may be accommodated by other mechanisms such as deformation twinning or fracture.

*jclayton@arl.army.mil

Electronic supplementary material is available at http://dx.doi.org/10.1098/rspa.2008.0281 or via http://journals.royalsociety.org.

Received 8 July 2008
Accepted 18 September 2008

Deformation twinning is thought to be preferred over slip in cases where resistances to dislocation glide are very large in certain directions (Hirth & Lothe 1982), often in crystals of non-cubic symmetry. Furthermore, twinning may be preferable to slip at low temperatures in cubic crystals, especially those with low stacking fault energy (Bernstein & Tadmor 2004). As reviewed by Christian & Mahajan (1995), a number of theories exist that describe twin nucleation and propagation. Here, deformation twinning is associated with irreversible shape deformation often attributed to the motion of partial dislocations and corresponding formation of stacking faults (Bilby & Crocker 1965; Christian & Mahajan 1995), although twinning in a more general sense may encompass a variety of energy invariant transformations of the lattice (Bhattacharya 1991). Although the general theory developed in this paper applies to any crystalline solid deformable via some combination of elasticity, slip and twinning, the present application of the theory focuses on ceramic crystals. As defined here, a ceramic crystal is an inorganic, non-metallic and ordered solid. Electronic structures of ceramics feature ionic and/or covalent bonds as opposed to metallic bonds found in ductile metals. The nature of interatomic forces in ionic and covalently bonded solids tends to correlate with a high Peierls barrier that inhibits dislocation motion at low temperatures (Friedel 1964).

Single crystals of the ceramic alumina (Al_2O_3) are known as corundum. The stable phase at room temperature and pressure is α-corundum, and although other phases exist (Holm *et al.* 1999), the term corundum hereafter refers to the α-phase. The crystallography of corundum can be described via either rhombohedral or hexagonal notation (Kronberg 1957). Corundum is centrosymmetric and hence does not exhibit the piezoelectric effect. Corundum that is red in colour, from elemental traces of chromium, is known as ruby, with the chromium content providing an increase in the tensile yield stress at high temperatures (Klassen-Neklyudova *et al.* 1970). Corundum of all other colours is called sapphire. Sapphire is very hard, with a value of 9 on Mohr's scale, and exhibits an extremely high Hugoniot elastic limit (HEL), with values in excess of 20 GPa for single crystals of certain orientations (Graham & Brooks 1971). Alumina's high hardness, high compressive strength and low mass density relative to steels render the ceramic a useful material for many engineering devices and systems. Single crystals of adequate purity are transparent, with widespread uses in optics and electronics. Experimental data quantifying the mechanical response of sapphire single crystals of various orientations and spanning a wide range of temperatures and strain rates are available (Graham & Brooks 1971; Tymiak & Gerberich 2007). While various kinetic relationships for slip (Lagerlof *et al.* 1994; Rodriguez *et al.* 2008) and twinning (Scott & Orr 1983) have been postulated to describe individual experiments, a more general model is needed to collectively explain the material's behaviour over a broad range of loading conditions encountered in practical applications.

The remainder of this paper is organized as follows. In §2, physical descriptions of elasticity, plasticity and twinning in crystalline solids are given, in order to clarify distinctions among the three mechanisms and provide sufficient basis for the theoretical framework of §3. This framework is general enough to apply to any crystalline solid that undergoes large deformations via elasticity, plasticity and/or mechanical twinning. In §4, the model is specialized to describe the behaviour of sapphire. Crystal structure, physical properties,

yield mechanisms, strain hardening, defect accumulation and irreversible volume changes associated with lattice defects are considered in turn.

The following notational scheme is used. Scalars and individual components of vectors and tensors are written in italic font, while vectors and tensors are written in bold-italic font. Einstein's summation convention applies for repeated indices. The $\cdot$ symbol denotes the scalar product ($\boldsymbol{a}\cdot\boldsymbol{b}=a^a b_a=a^1b_1+a^2b_2+a^3b_3$), while $\otimes$ indicates the outer product ($(\boldsymbol{a}\otimes\boldsymbol{b})^{ab}=a^a b^b$). Juxtaposition of second-rank tensors implies summation over one set of adjacent indices ($\boldsymbol{AB}=A^{ab}B_{bc}$). Summation over two sets of adjacent indices is denoted by : ($\boldsymbol{A:B}=A^{ab}B_{ab}$). Indices in parentheses are symmetric ($2A_{(ab)}=A_{ab}+A_{ba}$); indices in braces are antisymmetric ($2A_{[ab]}=A_{ab}-A_{ba}$). Superposed $\cdot$, T and -1 denote a material time derivative, transposition and matrix inversion. Subscripted commas denote partial coordinate differentiation.

2. Background: deformation mechanisms

(*a*) *Elasticity*

A crystal is said to deform elastically in the absence of generation or motion of defects. At the atomic scale, elastic deformation alters relative distances and/or orientations among neighbouring atoms within each crystallographic unit cell (Born & Huang 1954). Any resulting changes in interatomic forces produce mechanical stresses when the crystal is viewed as a continuous solid. Removal of mechanical stresses restores the original lattice without dissipation of energy; hence, elastic deformation is said to be thermodynamically reversible. Here, elastic deformation also includes changes in interatomic bond vectors induced by changes in temperature. Increases in thermal energy, i.e. local atomic vibrations, may correlate with the expansion of the lattice in the absence of mechanical stresses.

(*b*) *Plasticity*

Plastic deformation as defined here occurs via glide of dislocations of edge, screw and/or mixed character, including loops, and encompassing cross-slip but not climb. As dislocations travel through a region of the lattice, the shape of the material will change, but the interatomic bond vectors remain the same, so long as no defects are left behind within the region. Mechanical stresses are conventionally required to enact the net glide of dislocations (apart from random thermal fluctuations), for example resolved shear stresses must exceed the Peierls barrier in the context of lattice statics or Schmid's law in the context of continuum slip (Hirth & Lothe 1982). Plasticity is thermomechanically irreversible, since the reference shape of the material is not recovered upon removal of mechanical stresses, and heat is dissipated by moving dislocations as a result of lattice friction, phonon drag and other mechanisms (Kocks *et al.* 1975; Gilman 1979).

(*c*) *Twinning*

Deformation twinning results in two connected regions in the lattice separated by a twin boundary whose shape deformations differ by a simple shear. The original lattice is termed as the 'parent', while the sheared lattice is termed as the

'twin'. The atomic positions, and hence the corresponding lattice vectors between these atoms, within each region differ by a finite rotation, typically either a reflection or 180° rotation (Christian & Mahajan 1995), although more general relationships are possible. Nucleation and propagation of twins are thought to take place by one or more mechanisms, often involving the formation and motion of partial dislocations and atomic shuffles needed to maintain the orientation relationships between the twin and parent (Bilby & Crocker 1965). Deformation twinning is distinguished from plastic slip in that the former occurs by collective motion of defects, resulting in a quantized amount of shear that preserves the particular orientation relationship between the twin and parent. Another difference is that twinning is polar (i.e. unidirectional) while usually slip is not. Lattice geometry precludes twinning shears of equal magnitude and opposite directions on the same plane, while typically slip may occur in opposite directions on the same plane. The mechanical work of deformation twinning is dissipative, resulting from the defect motion associated with shearing. Possible energy storage is associated only with defects left behind in the lattice, for example those comprising the twin boundary. From continuum thermomechanics considerations, the driving force for twin propagation is the resolved shear stress in the direction of twinning shear. Detwinning, i.e. restoration of the twinned lattice to its original orientation, is possible, although is more applicable to phase transformations (Bhattacharya 1991) and less applicable to mechanical twinning of the kind considered here.

Twins are usually classified as type I, type II or compound. In centrosymmetric crystals, the lattice vectors in the twin and parent for a type I twin are related by either a reflection in the habit plane or rotation of 180° about the direction normal to this plane. For a type II twin, the lattice vectors are related by either a rotation of 180° about the shear direction or a reflection in the plane normal to the shear direction. The orthogonal transformation

$$\bar{\boldsymbol{Q}} = \begin{cases} 2\boldsymbol{m}_0 \otimes \boldsymbol{m}_0 - \mathbf{1} & \text{(type I)}, \\ 2\boldsymbol{s}_0 \otimes \boldsymbol{s}_0 - \mathbf{1} & \text{(type II)} \end{cases} \tag{2.1}$$

relates a lattice vector $\boldsymbol{a}_0$ in the parent to a lattice vector $\boldsymbol{a}$ in the twin via $\boldsymbol{a} = \bar{\boldsymbol{Q}}\boldsymbol{a}_0$. The unit normal to the habit plane is $\boldsymbol{m}_0$ and the direction of shear is $\boldsymbol{s}_0$. The rank-two unit tensor is denoted by $\mathbf{1}$. For a compound twin, both definitions in (2.1) are equivalent.

3. Continuum theory: nonlinear elasticity, slip and twinning

A constitutive framework for crystals undergoing large thermoelastic, plastic and twinning deformations is developed. The model is based upon principles of continuum mechanics and thermodynamics of single crystal behaviour, as described for example in Clayton (2005). Plastic deformation is limited to that resulting from dislocation glide, and twinning deformation is limited to mechanical twinning.

(*a*) *Kinematics*

A local volume element of crystalline material is identified by its reference coordinates $\boldsymbol{X}$. Let $\boldsymbol{x}=\boldsymbol{\varphi}(\boldsymbol{X},t)$ denote spatial coordinates of the element, with $\boldsymbol{\varphi}$ the motion. The deformation gradient $\boldsymbol{F}$ for the element is the tangent mapping

$$\boldsymbol{F} = T\boldsymbol{\varphi}_X = \partial \boldsymbol{x}/\partial \boldsymbol{X}, \tag{3.1}$$

decomposed multiplicatively into three terms

$$\boldsymbol{F} = \boldsymbol{F}^{\boldsymbol{E}}\bar{\boldsymbol{F}}^{\boldsymbol{I}}\boldsymbol{F}^{\boldsymbol{P}} = \boldsymbol{F}^{\boldsymbol{E}}\bar{\boldsymbol{F}}\,, \tag{3.2}$$

where $\boldsymbol{F}^{\boldsymbol{E}}$ accounts for recoverable thermoelastic deformation and rigid body rotation; $\bar{\boldsymbol{F}}^{\boldsymbol{I}} = \bar{J}^{1/3}\boldsymbol{F}^{\boldsymbol{I}}$ accounts for defect kinematics that alter the lattice; and $\boldsymbol{F}^{\boldsymbol{P}}$ accounts for lattice-preserving plastic slip. Twinning is modelled via the isochoric term $\boldsymbol{F}^{\boldsymbol{I}}$, and residual volume changes associated with defects are captured by the Jacobian determinant $\bar{J}$. The total irreversible deformation is $\bar{\boldsymbol{F}} = \bar{\boldsymbol{F}}^{\boldsymbol{I}}\boldsymbol{F}^{\boldsymbol{P}}$.

Introduced next are sets of contravariant and covariant vectors denoting directions and planes, respectively, for slip and twinning. When referred to the reference lattice prior to any reorientation by twinning, these are denoted by $\{\boldsymbol{s}_0^i, \boldsymbol{m}_0^i\}$ for each slip system i and $\{\boldsymbol{s}_0^j, \boldsymbol{m}_0^j\}$ for each twin system j. The total number of slip and twin systems is denoted by n and w, respectively. Reference shearing directions and plane normals are all of unit length, and each pair of contravariant shear direction and covariant plane normal is orthogonal

$$\begin{aligned} &\boldsymbol{s}_0^i\cdot\boldsymbol{m}_0^i = 0, \;\; |\boldsymbol{s}_0^i| = |\boldsymbol{m}_0^i| = 1 \;\; (\forall\, i = 1, \ldots, n);\\ &\boldsymbol{s}_0^j\cdot\boldsymbol{m}_0^j = 0, \;\; |\boldsymbol{s}_0^j| = |\boldsymbol{m}_0^j| = 1 \;\; (\forall\, j = 1, \ldots, w). \end{aligned} \tag{3.3}$$

During the course of twinning deformation, one or more parts (i.e. twins) of the volume element of crystal undergo a rotation relative to the parent. In a volume fraction of the crystal undergoing twinning via mode j, the slip directions and slip plane normals transform according to the usual rules for contravariant and covariant vectors, i.e.

$$\begin{aligned} &\boldsymbol{s}_{0j}^i = \bar{\boldsymbol{Q}}^j\boldsymbol{s}_0^i, \;\; \boldsymbol{m}_{0j}^i = \boldsymbol{m}_0^i\bar{\boldsymbol{Q}}^{jT}\\ &\qquad (\forall\; i = 1, \ldots, n \text{ slip systems};\;\; \forall\;\; j = 1, \ldots, w \text{ twin volumes}), \end{aligned} \tag{3.4}$$

where $\bar{\boldsymbol{Q}}^j$ is the rotation found from (2.1) corresponding to particular twin system j. For example, if j is a type I twin, $\bar{\boldsymbol{Q}}^j = 2\boldsymbol{m}_0^j\otimes\boldsymbol{m}_0^j - \mathbf{1}$, while if j is a type II twin, $\bar{\boldsymbol{Q}}^j = 2\boldsymbol{s}_0^j\otimes\boldsymbol{s}_0^j - \mathbf{1}$. Note from (3.4) that, within each twinned volume, the updated slip directions $\boldsymbol{s}_{0j}^i$ and slip plane normals $\boldsymbol{m}_{0j}^i$ remain orthogonal and of unit length for each i. For simplicity, successive twinning is not considered, which means that secondary twins do not form within already twinned regions and reorientation of the twinning systems $\{\boldsymbol{s}_0^j, \boldsymbol{m}_0^j\}$ is not considered. The rotation in (3.4) does not apply to the volume fraction of the grain comprising the parent. The thermoelastic deformation affects the lattice in the usual manner

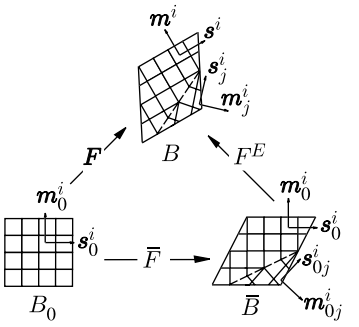

Figure 1. Deformations and slip system geometry for crystal deforming by elasticity, slip and twinning.

of crystal plasticity theory (Asaro 1983)

$$\begin{aligned}
&\boldsymbol{s}^i = \boldsymbol{F}^{\boldsymbol{E}}\boldsymbol{s}^i_0, \quad \boldsymbol{m}^i = \boldsymbol{m}^i_0\boldsymbol{F}^{\boldsymbol{E}-1} \quad (\forall\, i = 1, \ldots, n \in \text{ parent}),\\
&\boldsymbol{s}^i_j = \boldsymbol{F}^{\boldsymbol{E}}\boldsymbol{s}^i_{0j}, \quad \boldsymbol{m}^i_j = \boldsymbol{m}^i_{0j}\boldsymbol{F}^{\boldsymbol{E}-1} \quad (\forall\, i = 1, \ldots, n \in \text{ twins} \quad j = 1, \ldots, w),\\
&\boldsymbol{s}^j = \boldsymbol{F}^{\boldsymbol{E}}\boldsymbol{s}^j_0, \quad \boldsymbol{m}^j = \boldsymbol{m}^j_0\boldsymbol{F}^{\boldsymbol{E}-1} \quad (\forall\, j = 1, \ldots, w \in \text{ parent}).
\end{aligned} \tag{3.5}$$

Figure 1 depicts (3.1)–(3.5) for a crystal with a single slip system and a single twin. The multiplicative decomposition (3.2) implies a series of configurations of the material element. The reference configuration is labelled as B_0 with coordinates $\boldsymbol{X}$, the spatial configuration is labelled as B with coordinates $\boldsymbol{x}$ and the elastically unloaded intermediate configuration is labelled as $\bar{B}$. Since $\boldsymbol{F}^{\boldsymbol{E}-1}$ and $\bar{\boldsymbol{F}}$ are in general not integrable, continuous coordinates spanning $\bar{B}$ do not exist (Clayton *et al.* 2005). However, elastic and inelastic deformations act as tangent maps between configurations via $\boldsymbol{F}^{\boldsymbol{E}} : T\bar{B} \to TB$ and $\bar{\boldsymbol{F}} : TB_0 \to T\bar{B}$. In this illustration, the mappings $\bar{\boldsymbol{F}}^{\boldsymbol{I}}$ and $\boldsymbol{F}^{\boldsymbol{P}}$ comprising $\bar{\boldsymbol{F}}$ cannot be separately resolved owing to the effect of twinning on the orientation of the reference lattice.

The spatial velocity gradient following from (3.1) and (3.2) is

$$\begin{aligned}
\boldsymbol{L} = \dot{\boldsymbol{F}}\,\boldsymbol{F}^{-1} =& \dot{\boldsymbol{F}}^{\boldsymbol{E}}\boldsymbol{F}^{\boldsymbol{E}-1} + \boldsymbol{F}^{\boldsymbol{E}}\dot{\boldsymbol{F}}^{\boldsymbol{I}}\boldsymbol{F}^{\boldsymbol{I}-\boldsymbol{1}}\boldsymbol{F}^{\boldsymbol{E}-1}\\
&+ \boldsymbol{F}^{\boldsymbol{E}}\boldsymbol{F}^{\boldsymbol{I}}\dot{\boldsymbol{F}}^{\boldsymbol{P}}\boldsymbol{F}^{\boldsymbol{P}-1}\boldsymbol{F}^{\boldsymbol{I}-1}\boldsymbol{F}^{\boldsymbol{E}-1} + (1/3)\dot{\bar{J}}\bar{J}^{-1}\mathbf{1}.
\end{aligned} \tag{3.6}$$

The inelastic velocity gradient referred to configuration $\bar{B}$ is

$$\dot{\bar{\boldsymbol{F}}}\,\bar{\boldsymbol{F}}^{-1} = \boldsymbol{L}^{\boldsymbol{I}} + \bar{\boldsymbol{L}}^{\boldsymbol{P}} + (1/3)\dot{\bar{J}}\bar{J}^{-1}\mathbf{1}, \tag{3.7}$$

where

$$\boldsymbol{L}^{\boldsymbol{I}} = \dot{\boldsymbol{F}}^{\boldsymbol{I}}\boldsymbol{F}^{\boldsymbol{I}-1} = \sum_{j=1}^{w} \dot{f}^j\gamma^j\boldsymbol{s}^j_0 \otimes \boldsymbol{m}^j_0, \tag{3.8}$$

results from twinning shears, and

$$\bar{\boldsymbol{L}}^{\boldsymbol{P}} = (1-f_{\mathrm{r}})\sum_{i=1}^{n}\dot{\gamma}^i\boldsymbol{s}^i_0 \otimes \boldsymbol{m}^i_0 + \sum_{j=1}^{w}\left(f^j\sum_{i=1}^{n}\dot{\gamma}^i_j\boldsymbol{s}^i_{0j} \otimes \boldsymbol{m}^i_{0j}\right), \tag{3.9}$$

results from slip in both the parent and twinned regions of the crystal. In (3.8), γ^j is the predefined shear deformation associated with twin system j. In (3.9), $\dot{\gamma}^i$ is the slip rate on system i in the parent and $\dot{\gamma}^i_j$ is the slip rate on system i within reoriented twin fraction j. The volume fraction of crystal occupied by twin j, measured per unit volume in configuration $\bar{B}$, is labelled by the scalar $f^j \geq 0$, with rate $\dot{f}^j$ (Chin *et al.* 1969; Van Houtte 1978). The total volume fraction of twinned crystal is $f_{\mathrm{T}} = \sum f^j$, subject to the restriction $0 \leq f_{\mathrm{T}} \leq 1$. Detwinning is not considered; hence, $\dot{f}^j \geq 0$. In the interior summation within the rightmost term of (3.9), the slip directors and slip plane normals in the twinned regions are found according to (3.4), where the particular form of $\bar{\boldsymbol{Q}}^j$ corresponds to the twin with an associated value of f^j in the outer summation. Note that since for each slip or twin system, the shear directions and plane normals are orthogonal,

$$J^I \mathrm{tr}\boldsymbol{L}^{\boldsymbol{I}} = 0 \Rightarrow J^I = 1, \qquad J^I J^P \mathrm{tr}(\boldsymbol{L}^{\boldsymbol{I}} + \bar{\boldsymbol{L}}^{\boldsymbol{P}}) = 0 \Rightarrow J^P = 1, \tag{3.10}$$

upon assuming that at $t=0$, $\boldsymbol{F}^{\boldsymbol{I}} = \boldsymbol{F}^{\boldsymbol{P}} = \mathbf{1}$ and where $\mathrm{tr}\boldsymbol{A} = A^a_a$ for rank-two matrix $\boldsymbol{A}$. Thus, (3.8)–(3.10) reflect the isochoric nature of slip and twinning, and together with (3.2) and (3.6) require that all volume changes be accommodated thermoelastically via J^E and/or by defect generation via $\bar{J}$, such that

$$J = \sqrt{\det \boldsymbol{g}/\det \boldsymbol{G}}\, \det \boldsymbol{F} = J^E \bar{J}\,, \tag{3.11}$$

where $\boldsymbol{g}$ and $\boldsymbol{G}$ are metric tensors associated with coordinate systems in configurations B and B_0, with respective components $g_{ab} = \partial_a \boldsymbol{x} \cdot \partial_b \boldsymbol{x} = \boldsymbol{g}_a \cdot \boldsymbol{g}_b$ and $G_{AB} = \partial_A \boldsymbol{X} \cdot \partial_B \boldsymbol{X} = \boldsymbol{G}_A \cdot \boldsymbol{G}_B$. The residual volume change $\bar{J}$ arising from distributed defects such as dislocation lines follows from the notion that in nonlinear elasticity, the average strain of a body containing residual stress fields arising from internal displacement discontinuities need not vanish even if the traction on its external surfaces vanishes (Toupin & Rivlin 1960; Wright 1982). Here, only volume changes are considered, e.g. corresponding to random defect distributions imparting no preferred directions in residual strains, although more general treatments allowing for shape changes arising from the local elastic stress fields of crystal defects have been posited (Clayton *et al.* 2005). In §4*e*, a relationship between $\bar{J}$ and the dislocation density is given.

Two non-dimensional internal state variables are introduced to represent energetic changes associated with lattice defects. The first is a measure of the total line density of dislocations that accumulate with slip, $\xi = b\sqrt{\rho_{\mathrm{T}}}$, where b is a scalar Burgers vector—or a constant in the order of a lattice parameter for crystals containing dislocation families with different Burgers vectors—and ρ_{T} is the total length of such dislocations per unit volume in $\bar{B}$. The second is a measure of the total area density of twin boundaries, $\zeta = \sqrt{b\eta_{\mathrm{T}}}$, where η_{T} is the total area of twin boundaries per unit volume in $\bar{B}$.

(*b*) *Constitutive assumptions*

Let ρ and ρ_0 denote the mass density of the solid in current and reference configurations, respectively, related by $\rho_0 = \rho J$. Let $\bar{\rho} = \rho J^E = \rho_0 \bar{J}^{-1}$ denote the mass density in configuration $\bar{B}$. The Helmholtz free energy per unit volume in $\bar{B}$ is $\bar{\Psi} = \bar{\rho}\psi$, where ψ is the free energy per unit mass. The free energy exhibits the dependencies

$$\bar{\Psi} = \bar{\Psi}(\boldsymbol{E}^{\boldsymbol{E}}, \theta, \xi, \zeta, \{f^j\}), \tag{3.12}$$

where θ is the absolute temperature; ξ and ζ are respectively, related to the densities of dislocations and twin boundaries as discussed in §3*a*; the set $\{f^j\}$ includes each of the twin fractions, and

$$E^E_{\alpha\beta} = \frac{1}{2}\left(C^E_{\alpha\beta} - \delta_{\alpha\beta}\right) = \frac{1}{2}\left(F^{Ea}_{\cdot\alpha} g_{ab} F^{Eb}_{\cdot\beta} - \delta_{\alpha\beta}\right) \tag{3.13}$$

is a finite elastic strain tensor associated with the covariant elastic deformation tensor $\boldsymbol{C^E}$, with Cartesian metric $\delta_{\alpha\beta}$ used in configuration $\bar{B}$.

(*c*) *Thermodynamics*

Local forms of the balance of energy and dissipation inequality referred to the reference configuration are written respectively, as

$$\rho_0 \dot{e} = \boldsymbol{\Sigma} : \dot{\boldsymbol{E}} - \boldsymbol{\nabla}_0 \cdot \boldsymbol{Q} + \rho_0 r, \qquad \boldsymbol{\Sigma} : \dot{\boldsymbol{E}} - \rho_0(\dot{\psi} + \eta\dot{\theta}) - \frac{1}{\theta}\boldsymbol{\nabla}_0\theta \cdot \boldsymbol{Q} \geq 0. \tag{3.14}$$

Here, $e = \psi + \theta\eta$ is the internal energy per unit mass, with η the entropy per unit mass. The symmetric second Piola–Kirchhoff stress $\boldsymbol{\Sigma}$ is related to the first Piola–Kirchhoff stress $\boldsymbol{P}$ and the Cauchy stress $\boldsymbol{\sigma}$ by

$$\Sigma^{AB} = F^{-1A}_{\cdot a} P^{aB} = J F^{-1A}_{\cdot a} \sigma^{ab} F^{-1B}_{\cdot b}. \tag{3.15}$$

Also, $\boldsymbol{E} = (1/2)\boldsymbol{F}^{\mathrm{T}}\boldsymbol{F} - \boldsymbol{G}$ is the right Cauchy–Green strain; $\boldsymbol{\nabla}_0$ denotes a covariant derivative on B_0; $\boldsymbol{Q}$ is the heat flux vector; and r denotes other heat sources. The stress power per unit intermediate volume can be written as

$$\bar{J}^{-1}\Sigma^{AB}\dot{E}_{AB} = \left(J^E F^{E-1\beta}_{\cdot b}\sigma^{ab} g_{ca} F^{Ec}_{\cdot\alpha}\right)\left(F^{E-1\alpha}_{\cdot e} L^e_{\cdot d} F^{Ed}_{\cdot\beta}\right) = \bar{M}^{\cdot\beta}_{\alpha}\bar{L}^{\alpha}_{\cdot\beta}, \tag{3.16}$$

where $\bar{\boldsymbol{M}} = \boldsymbol{C^E}\bar{\boldsymbol{\Sigma}}$, $\bar{\boldsymbol{\Sigma}} = J^E \boldsymbol{F^{E-1}}\boldsymbol{\sigma}\boldsymbol{F^{E-T}}$, and

$$\bar{\boldsymbol{L}} = \boldsymbol{F^{E-1}}\boldsymbol{L}\boldsymbol{F^E} = \boldsymbol{F^{E-1}}\dot{\boldsymbol{F}}^{\boldsymbol{E}} + \boldsymbol{L^I} + \bar{\boldsymbol{L}}^{\boldsymbol{P}} + (1/3)\dot{\bar{J}}\bar{J}^{-1}\mathbf{1}. \tag{3.17}$$

The rate of free energy per unit intermediate volume is

$$\dot{\bar{\Psi}} = \frac{\mathrm{d}}{\mathrm{d}t}(\bar{\rho}\psi) = \bar{J}^{-1}\rho_0\left(\dot{\psi} - \dot{F}^{\alpha}_{\cdot A}\bar{F}^{-1A}_{\cdot\alpha}\psi\right) \tag{3.18}$$

and following from (3.17) and the symmetry properties of $\bar{\boldsymbol{\Sigma}}$ and $\dot{\boldsymbol{E}}^{\boldsymbol{E}}$,

$$\bar{M}^{\cdot\beta}_{\alpha}\bar{L}^{\alpha}_{\cdot\beta} = \bar{\Sigma}^{\beta\delta}\dot{E}^E_{\delta\beta} + \bar{M}^{\cdot\beta}_{\alpha}L^{I\alpha}_{\cdot\beta} + \bar{M}^{\cdot\beta}_{\alpha}\bar{L}^{P\alpha}_{\cdot\beta} + (1/3)\dot{\bar{J}}\,\bar{J}^{-1}\bar{M}^{\cdot\beta}_{\beta}. \tag{3.19}$$

Using the chain rule to expand the rate of $\bar{\Psi}$ of (3.12),

$$\dot{\bar{\Psi}} = \frac{\partial\bar{\Psi}}{\partial\boldsymbol{E}^{\boldsymbol{E}}} : \dot{\boldsymbol{E}}^{\boldsymbol{E}} + \frac{\partial\bar{\Psi}}{\partial\theta}\dot{\theta} + \frac{\partial\bar{\Psi}}{\partial\xi}\dot{\xi} + \frac{\partial\bar{\Psi}}{\partial\zeta}\dot{\zeta} + \frac{\partial\bar{\Psi}}{\partial f^j}\dot{f}^j, \tag{3.20}$$

with summation implied over w twin fractions j, the entropy inequality in (3.14) can be written as

$$\left(\bar{\boldsymbol{\Sigma}} - \frac{\partial\bar{\Psi}}{\partial\boldsymbol{E}^{\boldsymbol{E}}}\right) : \dot{\boldsymbol{E}}^{\boldsymbol{E}} - \left(\bar{N} + \frac{\partial\bar{\Psi}}{\partial\theta}\right)\dot{\theta} + \bar{\boldsymbol{\Pi}} : \left(\boldsymbol{L^I} + \bar{\boldsymbol{L}}^{\boldsymbol{P}} + \frac{\dot{\bar{J}}}{3\bar{J}}\mathbf{1}\right)$$
$$- \frac{\partial\bar{\Psi}}{\partial\xi}\dot{\xi} - \frac{\partial\bar{\Psi}}{\partial\zeta}\dot{\zeta} - \frac{\partial\bar{\Psi}}{\partial f^j}\dot{f}^j - \frac{1}{\theta}\bar{\boldsymbol{\nabla}}\theta \cdot \bar{\boldsymbol{q}} \geq 0, \tag{3.21}$$

where $\bar{N}=\bar{\rho}\eta$ is the entropy per unit intermediate volume; $\bar{\nabla}\theta=\nabla_0\theta\bar{\boldsymbol{F}}^{-1}$ is the intermediate temperature gradient; $\bar{\boldsymbol{q}}=\bar{J}^{-1}\bar{\boldsymbol{F}}\boldsymbol{Q}$ is the intermediate heat flux; and

$$\bar{\boldsymbol{\Pi}}=\bar{\boldsymbol{M}}-\bar{\Psi}\mathbf{1} \tag{3.22}$$

is a version of Eshelby's energy–momentum tensor (Eshelby 1975) mapped to configuration $\bar{B}$. Following standard arguments (Coleman & Noll 1963), stress–elastic strain and entropy–temperature relationships are deduced from (3.21) as

$$\bar{\boldsymbol{\Sigma}}=\frac{\partial\bar{\boldsymbol{\Psi}}}{\partial\boldsymbol{E}^{\boldsymbol{E}}},\quad \bar{N}=-\frac{\partial\bar{\Psi}}{\partial\theta},\quad \boldsymbol{\sigma}=J^{E-1}\boldsymbol{F}^{\boldsymbol{E}}\frac{\partial\bar{\Psi}}{\partial\boldsymbol{E}^{\boldsymbol{E}}}\boldsymbol{F}^{\boldsymbol{E}T},\quad \eta=-\bar{\rho}^{-1}\frac{\partial\bar{\Psi}}{\partial\theta}. \tag{3.23}$$

The final term on the left-hand side of (3.21) can be made non-negative upon prescription of the conduction law

$$\bar{\boldsymbol{q}}=-\bar{\boldsymbol{K}}\bar{\nabla}\theta,\qquad -\bar{\nabla}\theta\cdot\bar{\boldsymbol{q}}=\bar{\nabla}\theta\cdot\bar{\boldsymbol{K}}\bar{\nabla}\theta\geq 0, \tag{3.24}$$

where $\bar{\boldsymbol{K}}$ is a symmetric and positive definite matrix of thermal conductivity. Applying (3.23) and (3.24),

$$\bar{\boldsymbol{\Pi}}:\boldsymbol{L}^{\boldsymbol{I}}+\bar{\boldsymbol{\Pi}}:\bar{\boldsymbol{L}}^{\boldsymbol{P}}+\frac{\dot{\bar{J}}}{3\bar{J}}\mathrm{tr}\bar{\boldsymbol{\Pi}}\geq\frac{\partial\bar{\boldsymbol{\Psi}}}{\partial\xi}\dot{\xi}+\frac{\partial\bar{\boldsymbol{\Psi}}}{\partial\zeta}\dot{\zeta}+\frac{\partial\bar{\boldsymbol{\Psi}}}{\partial f^j}\dot{f}^j-\frac{1}{\theta}\bar{\nabla}\theta\cdot\bar{\boldsymbol{K}}\bar{\nabla}\theta, \tag{3.25}$$

is the reduced dissipation inequality. In the absence of temperature gradients, (3.25) requires that the energy dissipated by twinning, slip and residual volume changes must exceed the rate of energy storage associated with defects, specifically dislocations and twin boundaries. From (3.8)–(3.10), the energies dissipated from twinning and slip, respectively, can be written as

$$\bar{\boldsymbol{\Pi}}:\boldsymbol{L}^{\boldsymbol{I}}=\sum_{j=1}^{w}\bar{\tau}^j\dot{f}^j\gamma^j,\quad \bar{\boldsymbol{\Pi}}:\bar{\boldsymbol{L}}^{\boldsymbol{P}}=(1-f_{\mathrm{T}})\sum_{i=1}^{n}\bar{\tau}^i\dot{\gamma}^i+\sum_{j=1}^{w}\left(f^j\sum_{i=1}^{n}\bar{\tau}^i_j\dot{\gamma}^i_j\right), \tag{3.26}$$

where the driving forces are resolved stresses on each slip or habit plane, acting in the direction of shear

$$\bar{\tau}^j=J^E s^{ja}\sigma_a^{\cdot b}m^j_b,\qquad \bar{\tau}^i=J^E s^{ia}\sigma_a^{\bullet b}m^i_b,\qquad \bar{\tau}^i_j=J^E s^{ia}_j\sigma_a^{\bullet b}m^i_{jb}. \tag{3.27}$$

The specific heat capacity at constant elastic strain, measured per unit volume in $\bar{B}$, is introduced as

$$\bar{c}=\partial\bar{E}/\partial\theta=-\theta\partial^2\bar{\Psi}/\partial\theta^2, \tag{3.28}$$

where (3.23) has been used and $\bar{E}=\bar{\rho}e$ is the internal energy per intermediate volume. Multiplying the first of (3.14) by $\bar{J}^{-1}$, and using (3.15)–(3.20), (3.22)–(3.24) and (3.28), the energy balance can be written as

$$\begin{aligned}\bar{c}\dot{\theta}=\bar{\boldsymbol{\Pi}}:(\boldsymbol{L}^{\boldsymbol{I}}+\bar{\boldsymbol{L}}^{\boldsymbol{P}})+\left(\mathrm{tr}\bar{\boldsymbol{\Pi}}+\theta\frac{\partial\bar{\Psi}}{\partial\theta}\right)\frac{\dot{\bar{J}}}{3\bar{J}}-\theta\bar{\boldsymbol{\beta}}:\dot{\boldsymbol{E}}^{\boldsymbol{E}}+\breve{\nabla}\cdot\bar{\boldsymbol{K}}\bar{\nabla}\theta\\ -\left(\frac{\partial\bar{\Psi}}{\partial\xi}-\theta\frac{\partial^2\bar{\Psi}}{\partial\theta\partial\xi}\right)\dot{\xi}-\left(\frac{\partial\bar{\Psi}}{\partial\zeta}-\theta\frac{\partial^2\bar{\Psi}}{\partial\theta\partial\zeta}\right)\dot{\zeta}-\left(\frac{\partial\bar{\Psi}}{\partial f^j}-\theta\frac{\partial^2\bar{\Psi}}{\partial\theta\partial f^j}\right)\dot{f}^j,\end{aligned} \tag{3.29}$$

where non-mechanical sources r in (3.14) are assumed absent in (3.29) and hereafter. The stress–temperature coefficients are

$$\bar{\boldsymbol{\beta}}=-\partial^2\bar{\Psi}/\partial\theta\partial\boldsymbol{E}^{\boldsymbol{E}}, \tag{3.30}$$

and the notation for the heat conduction term in (3.29) is $\breve{\bar{\nabla}}_\alpha = \bar{\nabla}_\alpha + \bar{J}^{-1}(\bar{J}\,\bar{F}^{-1A}_{\ .\alpha})_{,A}$, with $\bar{\nabla}_\alpha = \nabla_{0A}\bar{F}^{-1A}_{\ .\alpha}$. Note that $\breve{\bar{\nabla}}_\alpha = \bar{\nabla}_\alpha$ when the compatibility conditions $\bar{F}^{\alpha}_{.[A,B]} = 0$ apply, in which case $(\partial\bar{J}/\partial\bar{F}^{\alpha}_{\ .A})_{,A} = 0$.

(*d*) *Representative free energy potential*

A more specific form of (3.12) is now specified for anisotropic crystals that may undergo large elastic deformations. The free energy is decomposed additively as

$$\bar{\Psi} = \bar{\Psi}^E(\boldsymbol{E}^{\boldsymbol{E}}, \theta, \{f^j\}) + \bar{Y}(\theta) + \bar{\Psi}^R(\xi, \zeta, \theta), \tag{3.31}$$

where $\bar{\Psi}^E$ accounts for the thermoelastic response; $\bar{Y}$ accounts for the purely thermal energy; and $\bar{\Psi}^R$ accounts for residual energy of lattice defects. The thermoelastic energy consists of three terms

$$\bar{\Psi}^E = \frac{1}{2}E^E_{\alpha\beta}\bar{\mathbb{C}}^{\alpha\beta\chi\delta}E^E_{\chi\delta} + \frac{1}{6}E^E_{\alpha\beta}\bar{\mathbb{C}}^{\alpha\beta\chi\delta\varepsilon\phi}E^E_{\chi\delta}E^E_{\varepsilon\phi} - \bar{\beta}^{\alpha\beta}E^E_{\alpha\beta}(\theta-\theta_0), \tag{3.32}$$

with the first term of (3.32) accounting for materially linear, but geometrically nonlinear, mechanical effects; the second accounting for nonlinear elastic effects important at high pressures (Brugger 1964; Graham & Brooks 1971); and the third accounting for thermoelastic coupling. Here, θ_0 is a constant temperature at which the lattice parameters exhibit their reference lengths, and the remaining coefficients in (3.32) consist of partial derivatives of the free energy at null elastic strain

$$\bar{\mathbb{C}}^{\alpha\beta\chi\delta} = \left.\frac{\partial^2\bar{\Psi}^E}{\partial E^E_{\alpha\beta}\partial E^E_{\chi\delta}}\right|_{\boldsymbol{E}^{\boldsymbol{E}}=\boldsymbol{0}},\quad \bar{\mathbb{C}}^{\alpha\beta\chi\delta\varepsilon\phi} = \left.\frac{\partial^3\bar{\Psi}^E}{\partial E^E_{\alpha\beta}\partial E^E_{\chi\delta}\partial E^E_{\varepsilon\phi}}\right|_{\boldsymbol{E}^{\boldsymbol{E}}=\boldsymbol{0}},\quad \bar{\beta}^{\alpha\beta} = -\left.\frac{\partial^2\bar{\Psi}^E}{\partial\theta\partial E^E_{\alpha\beta}}\right|_{\boldsymbol{E}^{\boldsymbol{E}}=\boldsymbol{0}}. \tag{3.33}$$

Coefficients in (3.33) may depend on temperature; when measured at a particular temperature, these are referred to as isothermal elastic constants. In anisotropic solids, the coefficients in (3.33) depend upon the orientation of the lattice in configuration $\bar{B}$. When twinning is involved, the orientations of the original reference lattice (parent) and each twinned region differ. It is assumed that the elastic deformation $\boldsymbol{F}^{\boldsymbol{E}}$ and strain $\boldsymbol{E}^{\boldsymbol{E}}$ act uniformly over the parent and twins comprising each volume element. The energy (3.32) is thus partitioned into contributions from the parent and each twin

$$\begin{aligned}\bar{\Psi}^E =& \frac{1}{2}(1-f_{\mathrm{T}})E^E_{\alpha\beta}\bar{\mathbb{C}}^{\alpha\beta\chi\delta}_0E^E_{\chi\delta} + \frac{1}{6}(1-f_{\mathrm{T}})E^E_{\alpha\beta}\bar{\mathbb{C}}^{\alpha\beta\chi\delta\varepsilon\phi}_0E^E_{\chi\delta}E^E_{\varepsilon\phi}\\ &-(1-f_{\mathrm{T}})\bar{\beta}^{\alpha\beta}_0E^E_{\alpha\beta}(\theta-\theta_0) + \sum_{j=1}^{w}f^j\left(\frac{1}{2}E^E_{\alpha\beta}\bar{\mathbb{C}}^{\alpha\beta\chi\delta}_{jT}E^E_{\chi\delta}\right.\\ &\left.+\frac{1}{6}E^E_{\alpha\beta}\bar{\mathbb{C}}^{\alpha\beta\chi\delta\varepsilon\phi}_{jT}E^E_{\chi\delta}E^E_{\varepsilon\phi} - \bar{\beta}^{\alpha\beta}_{jT}E^E_{\alpha\beta}(\theta-\theta_0)\right),\end{aligned} \tag{3.34}$$

where $\bar{\mathbb{C}}^{\alpha\beta\chi\delta}_0$, $\bar{\mathbb{C}}^{\alpha\beta\chi\delta\varepsilon\phi}_0$ and $\bar{\beta}^{\alpha\beta}_0$ refer to coefficients for the parent lattice, and where for each twin j (Kalidindi 1998),

$$\begin{aligned}\bar{\mathbb{C}}^{\alpha\beta\chi\delta}_{jT} = \bar{Q}^{\ j\alpha}_{.\varepsilon}\bar{Q}^{\ j\beta}_{.\phi}\bar{Q}^{\ j\chi}_{.\varphi}\bar{Q}^{\ j\delta}_{.\gamma}\bar{\mathbb{C}}^{\varepsilon\phi\varphi\gamma}_0,\quad \bar{\mathbb{C}}^{\alpha\beta\chi\delta\varepsilon\phi}_{jT} = \bar{Q}^{\ j\alpha}_{.\varphi}\bar{Q}^{\ j\beta}_{.\gamma}\bar{Q}^{\ j\chi}_{.\eta}\bar{Q}^{\ j\delta}_{.\iota}\bar{Q}^{\ j\varepsilon}_{.\kappa}\bar{Q}^{\ j\phi}_{.\lambda}\bar{\mathbb{C}}^{\varphi\gamma\eta\iota\kappa\lambda}_0,\\ \bar{\beta}^{\alpha\beta}_{jT} = \bar{Q}^{\ j\alpha}_{.\chi}\bar{Q}^{\ j\beta}_{.\delta}\bar{\beta}^{\chi\delta}_0.\end{aligned} \tag{3.35}$$

The stress–strain–temperature relationships followed from (3.23) and (3.31)–(3.34) are

$$\bar{\Sigma}^{\alpha\beta} = \bar{\mathbb{C}}^{\alpha\beta\chi\delta} E^E_{\chi\delta} + \frac{1}{2}\bar{\mathbb{C}}^{\alpha\beta\chi\delta\varepsilon\phi} E^E_{\chi\delta} E^E_{\varepsilon\phi} - \bar{\beta}^{\,\alpha\beta}(\theta - \theta_0), \tag{3.36}$$

where the effective coefficients

$$\bar{\mathbb{C}}^{\alpha\beta\chi\delta} = (1 - f_{\mathrm{T}})\bar{\mathbb{C}}^{\alpha\beta\chi\delta}_0 + \sum_{j=1}^{w} f^j \bar{\mathbb{C}}^{\alpha\beta\chi\delta}_{jT}, \quad \bar{\mathbb{C}}^{\alpha\beta\chi\delta\varepsilon\phi} = (1 - f_{\mathrm{T}})\bar{\mathbb{C}}^{\alpha\beta\chi\delta\varepsilon\phi}_0 + \sum_{j=1}^{w} f^j \bar{\mathbb{C}}^{\alpha\beta\chi\delta\varepsilon\phi}_{jT},$$
$$\bar{\beta}^{\,\alpha\beta} = (1 - f_{\mathrm{T}})\bar{\beta}^{\,\alpha\beta}_0 + \sum_{j=1}^{w} f^j \bar{\beta}^{\,\alpha\beta}_{jT}. \tag{3.37}$$

From (3.37), the rationale for inclusion of twin fractions in free energy functions (3.12) and (3.31) is now clear: the effective thermoelastic moduli depend on the evolving twin fractions. The associated rate of thermoelastic free energy change is

$$\frac{\partial \bar{\Psi}^E}{\partial f^j}\dot{f}^j = \bar{A}_j \dot{f}^j, \quad \bar{A}_j = \frac{1}{2} E^E_{\alpha\beta}\left(\bar{\mathbb{C}}^{\alpha\beta\chi\delta}_{jT} - \bar{\mathbb{C}}^{\alpha\beta\chi\delta}_0\right) E^E_{\chi\delta} + \frac{1}{6} E^E_{\alpha\beta}\left(\bar{\mathbb{C}}^{\alpha\beta\chi\delta\varepsilon\phi}_{jT} - \bar{\mathbb{C}}^{\alpha\beta\chi\delta\varepsilon\phi}_0\right)$$
$$\times E^E_{\chi\delta} E^E_{\varepsilon\phi} - \left(\bar{\beta}^{\,\alpha\beta}_{jT} - \bar{\beta}^{\,\alpha\beta}_0\right) E^E_{\alpha\beta}(\theta - \theta_0), \tag{3.38}$$

with summation applied over j. Consider a situation in which strains $E^E_{\alpha\beta} = \bar{\alpha}_{\alpha\beta}(\theta - \theta_0)$ arise from temperature change. The following relationship emerges between the thermal stress, thermal expansion ($\bar{\alpha}_{\alpha\beta}$) and elasticity coefficients

$$\bar{\beta}^{\,\alpha\beta} = \bar{\mathbb{C}}^{\alpha\beta\chi\delta}\bar{\alpha}_{\chi\delta} + \frac{1}{2}\bar{\mathbb{C}}^{\alpha\beta\chi\delta\varepsilon\phi}\bar{\alpha}_{\chi\delta}\bar{\alpha}_{\varepsilon\phi}(\theta - \theta_0). \tag{3.39}$$

Note that $\bar{\mathbb{C}}^{\alpha\beta\chi\delta} = \bar{\mathbb{C}}^{(\alpha\beta)(\chi\delta)}$, $\bar{\mathbb{C}}^{\alpha\beta\chi\delta\varepsilon\phi} = \bar{\mathbb{C}}^{(\alpha\beta)(\chi\delta)(\varepsilon\phi)}$ and $\bar{\beta}^{\,\alpha\beta} = \bar{\beta}^{\,(\alpha\beta)}$ follow automatically from (3.33). The Voigt notation (Brugger 1964) exploits the symmetry of the elastic stress $\bar{\boldsymbol{\Sigma}}$, elastic strain $\boldsymbol{E^E}$ and these coefficients, with pairs of indices $11 \to 1, 22 \to 2, 33 \to 3, 23 \to 4, 13 \to 5$ and $12 \to 6$ and $\bar{\Sigma}^{\alpha\beta} \to \bar{\Sigma}_A, 2E^E_{\alpha\beta} \to E^E_A(1 + \delta_{\alpha\beta})$, with Greek indices ($\alpha, \beta = 1, 2, 3$) and capital indices ($A = 1, 2, \ldots, 6$). Relation (3.36) then can be expressed compactly as

$$\bar{\Sigma}_A = C_{AB}E^E_B + \frac{1}{2}C_{ABC}E^E_B E^E_C - \bar{\beta}_A(\theta - \theta_0), \tag{3.40}$$

where C_{AB} and C_{ABC} are the second- and third-order elastic coefficients and summation proceeds over duplicate covariant indices. The thermal energy in (3.31) is prescribed as (Clayton 2005)

$$\bar{Y} = -\bar{c}\theta \ln(\theta/\theta_0). \tag{3.41}$$

Finally, the residual energy of (3.31) is specified as

$$\bar{\Psi}^R = \frac{1}{2}\mu\left(\kappa_1\xi^2 + \kappa_2\zeta^2 + \kappa_3\xi^2\zeta^2\right), \tag{3.42}$$

where μ is an elastic shear modulus that may depend on temperature and κ_1, κ_2 and κ_3 are dimensionless constants that scale the energies associated with each internal variable. Recalling from §3*a* that $\xi = b\sqrt{\rho_{\mathrm{T}}}$, the first term on the right-hand side of

(3.42) provides a linear dependence of residual energy on the line density of dislocations, following Clayton (2005) and references therein. Simple arguments then show that $2W_{\mathrm{D}}=\kappa_1\mu b^2$, where W_{D} is the total energy per unit line length of dislocations, including self- and interaction energies, core energy and stacking fault energy if the dislocations are partial. Recalling that $\zeta=\sqrt{b\eta_{\mathrm{T}}}$, the second term provides a linear dependence of residual energy on the area per unit volume of twin boundaries η_{T}. Similarly, $2W_{\mathrm{T}}=\kappa_2\mu b$, where W_{T} is the twin boundary energy per unit area. Often, $2W_{\mathrm{T}}\sim W_{\mathrm{SF}}$, where W_{SF} is the intrinsic or extrinsic stacking fault energy (Hirth & Lothe 1982; Bernstein & Tadmor 2004). The third term accounts for interaction energies between twin boundaries and dislocations. Alternative forms of (3.42) are of course possible and can be introduced as needed for particular materials. The rate of temperature increase (3.29) can now be written as

$$\bar{c}\dot{\theta}=\beta' W^P+\theta\left(\frac{\partial\bar{\Psi}}{\partial\theta}\frac{\dot{\bar{J}}}{3\bar{J}}-\bar{\boldsymbol{\beta}}:\boldsymbol{\dot{E}}^{\boldsymbol{E}}\right)+\breve{\nabla}\cdot\bar{\boldsymbol{K}}\bar{\nabla}\theta, \tag{3.43}$$

where

$$\beta'=1-\left[\left(\mu-\theta\frac{\partial\mu}{\partial\theta}\right)\left(\frac{b^2}{2}\left(\kappa_1+\kappa_3\frac{\eta_{\mathrm{T}}}{\sqrt{\rho_{\mathrm{T}}}}\right)\dot{\rho}_{\mathrm{T}}+\frac{b}{2}\left(\kappa_2+\kappa_3 b^{3/2}\frac{\rho_{\mathrm{T}}}{\sqrt{\eta_{\mathrm{T}}}}\right)\dot{\eta}_{\mathrm{T}}\right)+\left(\bar{A}_j-\theta\frac{\partial\bar{A}_j}{\partial\theta}\right)\dot{f}^j\right]W^{P-1} \tag{3.44}$$

is often called the Taylor–Quinney parameter (Taylor & Quinney 1934), such that $1-\beta'$ is the ratio of inelastic stress power $W^P=\bar{\boldsymbol{\Pi}}:(\boldsymbol{L}^{\boldsymbol{I}}+\bar{\boldsymbol{L}}^{\boldsymbol{P}}+(1/3)\dot{\bar{J}}\bar{J}^{-1}\mathbf{1})$ converted to residual elastic energy in the lattice.

(e) *Kinetics*

Here, rate-dependent, i.e. viscoplastic, relationships describe shearing associated with slip (Hutchinson 1976; Asaro 1983) and twinning (Kalidindi 1998). These kinetic equations read as

$$\dot{\gamma}^i=\dot{\gamma}_S\left|\frac{\bar{\tau}^i}{\bar{g}^i}\right|^m\frac{\bar{\tau}^i}{|\bar{\tau}^i|},\qquad \dot{\gamma}^i_j=\dot{\gamma}_S\left|\frac{\bar{\tau}^i_j}{\bar{g}^i_j}\right|^m\frac{\bar{\tau}^i_j}{|\bar{\tau}^i_j|},\qquad \dot{f}^j=\frac{\dot{\gamma}_T}{\gamma^j}\left|\frac{\langle\bar{\tau}^j\rangle}{\bar{g}^j}\right|^p. \tag{3.45}$$

In (3.45), $\dot{\gamma}_S$ and $\dot{\gamma}_T$ are material parameters with dimensions of $1/t$; m and p are dimensionless parameters; and $\bar{g}^i$ and $\bar{g}^j$ are evolving resistances—positive scalars with dimensions of stress—to deformation in the parent by slip on system i and twinning on system j, respectively. In the second of (3.45), $\bar{g}^i_j$ denote resistances on slip system i within reoriented twin j. In the third of (3.45), $2\langle\bar{\tau}^j\rangle=\bar{\tau}^j+|\bar{\tau}^j|$. From (3.26) and (3.45), these rates are always dissipative since for each slip system, $\bar{\tau}^i\dot{\gamma}^i\geq 0$ and $\bar{\tau}^i_j\dot{\gamma}^i_j\geq 0$ and for each twin, $\dot{f}^j\langle\bar{\tau}^j\rangle\gamma^j\geq 0$. Because $\dot{f}^j=0$ for $\bar{\tau}^j\leq 0$, the unidirectional nature of twinning is respected. In the limit $m\to\infty$ or $p\to\infty$, rate-independent behaviour is attained. In a general

sense, slip and twin resistances evolve as

$$\dot{\bar{g}}^i = \dot{\bar{g}}^i(\boldsymbol{E}^{\boldsymbol{E}}, \theta, \xi, \zeta, \{f^j\}, \{\bar{g}\}), \qquad \dot{\bar{g}}^i_j = \dot{\bar{g}}^i_j(\boldsymbol{E}^{\boldsymbol{E}}, \theta, \xi, \zeta, \{f^j\}, \{\bar{g}\}),$$

$$\dot{\bar{g}}^j = \dot{\bar{g}}^j(\boldsymbol{E}^{\boldsymbol{E}}, \theta, \xi, \zeta, \{f^j\}, \{\bar{g}\}), \tag{3.46}$$

where the rates depend not only on the set of state variables that explicitly enter the free energy (3.12), but also on the set of hidden variables $\{\bar{g}\} = \{\bar{g}^i, \bar{g}^j, \bar{g}^i_j\}$ with $i=1, \ldots, n$ and $j=1, \ldots, w$. Evolution equations for ξ and ζ, reflecting densities of dislocations and twin boundaries, complete the model. Analogous to hardening in (3.46), generic evolution equations are written as

$$\dot{\xi} = \dot{\xi}(\boldsymbol{E}^{\boldsymbol{E}}, \theta, \xi, \zeta, \{f^j\}, \{\bar{g}\}), \quad \dot{\zeta} = \dot{\zeta}(\boldsymbol{E}^{\boldsymbol{E}}, \theta, \xi, \zeta, \{f^j\}, \{\bar{g}\}). \tag{3.47}$$

Possible impedances of slip or twinning via slip–slip interactions, slip–twin interactions and twin–twin interactions entering (3.46) may depend in a complex manner on a number of factors, including geometric relationships between interacting systems, temperature, crystal structure and defect content (Christian & Mahajan 1995; Kalidindi 1998; Castaing *et al.* 2002; Wu *et al.* 2007). The theory is applicable over a potentially wide temperature range via dependence of initial values of resistances to slip and twinning (i.e. initial values of $\{\bar{g}\}$ in kinetic equations (3.45)) on temperature; in addition, these variables evolve with the history of deformation and temperature according to (3.46).

4. Application: sapphire single crystals

The framework of §3 is specialized to describe sapphire. Crystal structure, physical properties, initial yield mechanisms, strain hardening, defect accumulation and residual volume changes are considered. Whenever possible, experimental data motivate aspects of the model and provide associated parameters.

(*a*) *Crystal structure and properties*

The atomic structure of sapphire is depicted in terms of the Al nuclei in figure 2, following Kronberg (1957). The fundamental unit cell is rhombohedral (lattice parameter $a_0 = 0.512$ nm, bond angle 55.3°). The hexagonal unit cell, while consisting of more atoms, is convenient for describing mechanical behaviour. Two types of hexagonal cells are encountered in the literature. One is the morphological cell shown in figure 2*a*, consisting of three layers of Al cations each two-third full, with a close-packed full layer of O anions in between each layer of Al cations. The Al nuclei occupy octahedral interstitial sites between each hexagonal layer of O atoms (Kronberg 1957). The morphological hexagonal lattice parameters are $A = 0.475$ nm and $C_{\mathrm{M}} = 0.649$ nm. Figure 2*b* is of the structural cell, consisting of a second stack of each of the three layers of Al cations and O anions, differing from the morphological unit cell by a rotation of 180° about the *c*-axis [0001]. The lattice parameters of the structural hexagonal cell are $A' = 0.475$ nm and $C_{\mathrm{S}} = 2C_{\mathrm{M}} = 1.297$ nm, as shown in figure 2. Elastic constants are listed in table 1 (in the electronic supplementary material); because sapphire has trigonal symmetry,

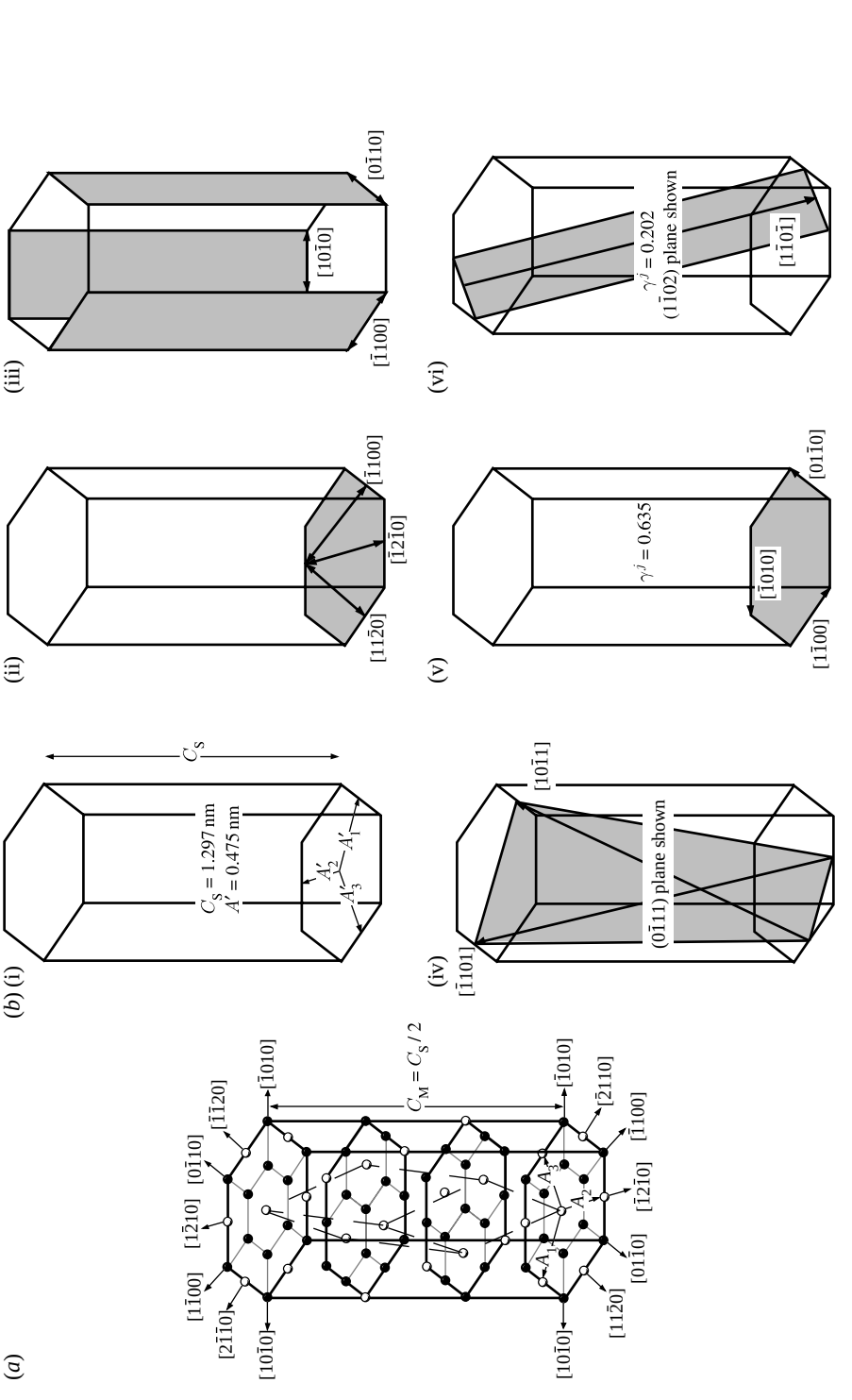

Figure 2. (*a*) Morphological unit cell (black circles, Al cation; white circles, Al vacancy; black solid lines, hexagonal; dashed lines, rhombohedral) and (*b*) prominent slip and twin systems in structural unit cell notation. ((i) Structural unit cell, (ii) basal slip, (iii) prism slip, (iv) pyramidal slip, (v) basal twinning, (vi) rhombohedral twinning.)

rotations of 180° about the *c*-axis do not fall within the point group of symmetry operations for the crystal. Hence, the signs of C_{14} and several of the third-order constants depend upon the choice of unit cell (Winey *et al.* 2001). In table 1 and henceforth, all properties are referred to the structural unit cell. The full matrices of anisotropic elastic coefficients in (3.40) are populated from the six independent second-order coefficients and 14 independent third-order coefficients using the scheme of Teodosiu (1982), for example. Relevant bulk physical properties with supporting references are listed in table 2 (in the electronic supplementary material).

Prominent slip and twin systems are listed in tables 3 and 4 (in the electronic supplementary material), respectively, and are illustrated in figure 2. While a number of different families of pyramidal systems are crystallographically conceivable (Snow & Heuer 1973), quantitative yield data seem scarce except for the $<\bar{1}101>\{10\bar{1}1\}$ systems, with available data limited to tensile deformation of whiskers at temperatures in excess of 2000 K (Tressler & Barber 1974). While basal and prism slip can occur in either direction for a given system, pyramidal slip is thought unidirectional (Heuer *et al.* 1998) and only occurs when the resolved shear stress acts in a positive sense with respect to the *c*-axis, e.g. tensile loading along [0001]. Twinning is also unidirectional; for example, rhombohedral twinning occurs only when the resolved shear stress acts in a negative sense with respect to the *c*-axis, e.g. compressive loading along [0001]. Thus, pure tensile deformation along [0001] can only be accommodated by pyramidal slip, elasticity or fracture, while pure compression along [0001] can only be accommodated by rhombohedral twinning, elasticity or fracture. The slip directions for unidirectional mechanisms are tabulated here such that the resolved shear stress for a given slip or twin system must be positive to enact shear on that system. Atomistic simulations of hypervelocity impact of sapphire have predicted basal and pyramidal slip and basal and rhombohedral twinning (Zhang *et al.* 2007). Bourne *et al.* (2007) observed prism and basal dislocations, twins, cleavage fracture and grain boundary fracture in specimens recovered from impact experiments on polycrystalline alumina, with activity or inactivity of certain mechanisms dependent on the impact stress.

Quantification of resistances for slip, twinning and fracture in sapphire remains an area of active research (Tymiak & Gerberich 2007). Fundamental arguments based on elasticity theory and lattice periodicity provide order-of-magnitude estimates for critical shear stresses that will be refined upon examination of experimental data. The isotropic Peierls stress (Peierls 1940) has been deemed useful for describing basal and prism slip in sapphire (Farber *et al.* 1993)

$$\tau_C = \frac{2\mu}{K}\exp\left(\frac{-2\pi d}{Kb}\right), \qquad K = \begin{cases} 1-\nu \text{ (edge dislocation)} \\ 1 \text{ (screw dislocation)} \end{cases} \quad \text{(slip)}, \tag{4.1}$$

where d is the spacing between slip planes and ν is Poisson's ratio. Eshelby (1949) derived expressions for anisotropic crystals; however, owing to their complexity, the need for consideration of the orientation of the dislocation line with respect to the lattice vectors and limitations of the sinusoidal interatomic potential used in the derivations, the anisotropic solutions are usually not considered, and are not pursued here. Table 5 (in the electronic supplementary material) lists the

Peierls stresses for sapphire; note that partial Burgers vectors are involved for prism slip, leading to a lower Peierls stress and a preference over basal slip at low temperatures (Lagerlof *et al.* 1994), although the original treatment of Peierls (1940) did not consider partials. For these computations, the rhombohedral shear modulus at room temperature is used as an estimate (table 2), along with the effective Poisson's ratio for alumina, $\nu = 0.24$ (Holm *et al.* 1999). The expression below has been postulated for twin nucleation (Hirth & Lothe 1982; Lagerlof *et al.* 1994)

$$\tau_C = W_{\mathrm{SF}}/b \quad \text{(twin nucleation)}, \tag{4.2}$$

recalling that W_{SF} is the stacking fault energy associated with partial dislocations of Burgers vector b responsible for twinning on the system of interest. Table 6 (in the electronic supplementary material) lists corresponding values for nucleation of basal and rhombohedral twins. A theoretical first-order estimate for shear fracture is (Frenkel 1926)

$$\tau_C = \mu b/(2\pi d) \quad \text{(shear fracture)}, \tag{4.3}$$

with values listed in table 7 (in the electronic supplementary material) for possible fracture planes in sapphire. Experiments indicate that the preferred cleavage planes are $\{10\bar{1}0\}$ prism planes and $\{\bar{1}012\}$ rhombohedral planes (Wiederhorn 1969; Azhdari & Nemat-Nasser 1998). The prism planes listed in table 7 are of the type $\{10\bar{1}0\}$, and hence comprise a different family than the $\{11\bar{2}0\}$ prism planes considered for slip in tables 3 and 5 and figure 2. Approximation (4.3) does not account for electrostatic forces in ionic crystals apart from their influence on the shear modulus, and hence neglects the strong Coulomb forces contributing to the high fracture energy of the {0001} planes, relative to the prism and rhombohedral planes, in sapphire (Wiederhorn 1969). Experimental measurements of cohesive energy or cleavage strength of $\{10\bar{1}1\}$ pyramidal planes are not available. Owing to sapphire's brittle nature at low temperatures, measurements of the yield mechanisms corresponding to (4.1)–(4.3) must occur at high pressures that suppress tensile fracture, e.g. indentation (Tymiak & Gerberich 2007) or confined compression (Graham & Brooks 1971; Castaing *et al.* 1981; Scott & Orr 1983; Lankford *et al.* 1998). Graham & Brooks (1971) suggested that shear failure via attainment of the theoretical strength (4.3) could occur in shock-loaded sapphire.

(*b*) *Thermoelasticity and critical shear stresses in uniaxial strain*

An analysis of the thermoelastic response of sapphire under adiabatic uniaxial strain boundary conditions enables consideration of the behaviour of oriented crystals up to the yield point or HEL. Driving forces for slip, twinning and fracture can be computed and compared with (4.1)–(4.3) and observations from shock physics experiments (Barker & Hollenbach 1970; Graham & Brooks 1971; Chen & Howitt 1998; Reinhart *et al.* 2006) to provide more suitable estimates for yield and failure criteria. This analysis also provides insight into which inelastic deformation mechanisms are most likely responsible for macroscopic yielding in shock physics experiments. In conventional plate impact experiments, the sequence of activity of yield and fracture mechanisms can usually only be inferred indirectly (Bourne *et al.* 2007), since visual characterization of defects (e.g. microscopy of dislocations, twins and micro-cracks) is generally not

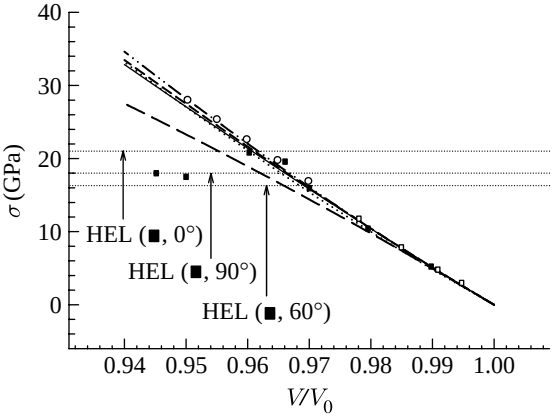

Figure 3. Axial Cauchy stress for single crystals: elasticity predictions and shock physics experiments (solid line, 0° nonlinear elasticity; dotted line, 60° nonlinear elasticity; short-dashed line, 90° nonlinear elasticity; dot-dashed line, rhombohedral nonlinear elasticity; long-dashed line, 0° linear elasticity; white squares, Barker & Hollenbach (0°); black squares, Graham & Brooks (0°, 60° and 90°); white circles, Reinhart *et al.* (0°)).

possible *in situ*, but rather is conducted on recovered specimens that fracture on tensile release, if not during the impact process. Stress-induced phase transformations are thought to occur only at very high pressures (approx. 79 GPa; Reinhart *et al.* 2006) and are not considered.

For uniaxial straining along the Cartesian three-axis, the deformation gradient (3.1) is $\boldsymbol{F}=\mathbf{1}+(\Delta V/V_0)\boldsymbol{g}_3\otimes\boldsymbol{G}^3$, where $\Delta V=V-V_0$ is the volume change and V_0 is the reference volume of the crystal. Thermoelastic responses are computed for crystals oriented with respect to the loading axis at 0° (along [0001]), 60° (along $[11\bar{2}3]$) and 90° (along $[\bar{1}2\bar{1}0]$), and with the loading axis normal to a rhombohedral plane (along $[\bar{1}012]$). Shown in figure 3 is the axial stress component $\sigma=\sigma^{33}$ computed for each orientation, accounting for anisotropic nonlinear elasticity and thermal expansion. Also shown is the response for a 0°-oriented crystal computed using only the second-order elastic constants, i.e. $C_{ABC}=0$ in (3.40), and labelled 'linear elasticity'. Experimental data points are provided from the aforementioned sources, and dotted horizontal lines indicate maximum observed HEL values quoted by Graham & Brooks (1971). Among the nonlinear elastic predictions, minute differences in stress arise between crystals of different orientations below the HEL. Among corresponding experiments, differences among crystals of different orientations are not discernable in the elastic regime (Graham & Brooks 1971). From figure 3, nonlinear elasticity provides an adequate match to the experimental results for $V/V_0\geq 0.95$, while linear elasticity is inadequate for volume changes $V/V_0<0.98$. For each orientation, temperature rises predicted by the nonlinear theory from an initial temperature of $\theta_0=300$ K were of the order of 20 K at $V/V_0=0.95$. In the experiments, significant stress drops occur for $V/V_0<0.95$; comparison with the hydrostat of sapphire indicates a significant loss of shear strength above the HEL, pointing to possible fracture processes. Values of the post-HEL shear strength have been reported in the range of 4.0–6.0 GPa (Graham & Brooks 1971; Munson & Lawrence 1979; Reinhart *et al.* 2006).

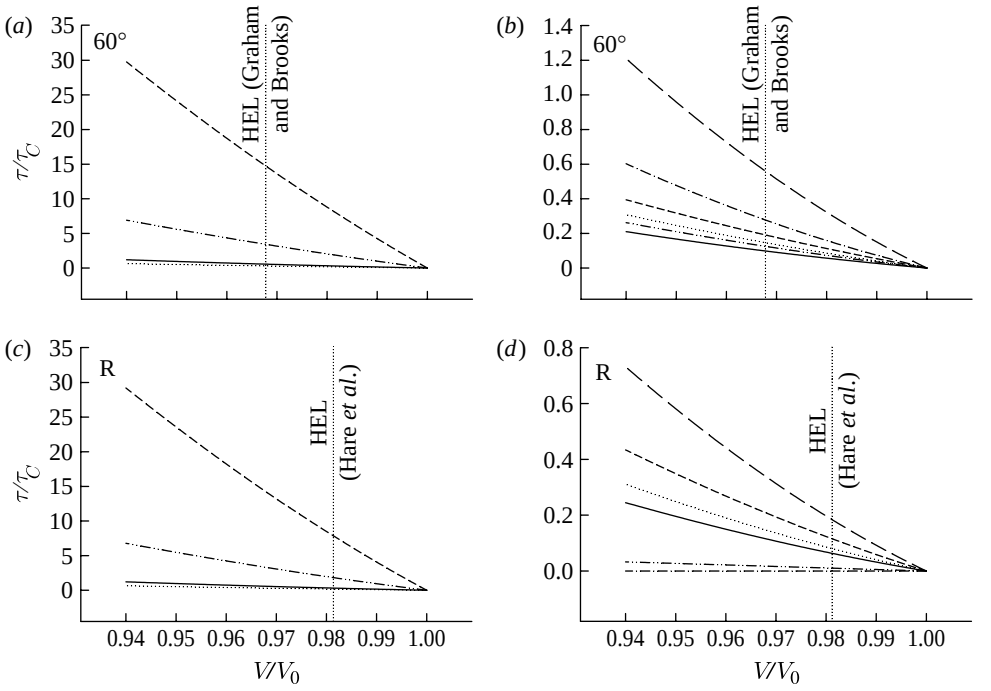

Figure 4. Ratio of maximum shear stress computed from nonlinear elasticity to theoretical estimates of Peierls stress, shear fracture strength or twin nucleation stress: (*a*,*b*) 60° orientation; dotted lines, HEL (Graham & Brooks 1971) (*c*,*d*) rhombohedral orientation; dotted lines, HEL (Hare *et al.* 2002). (*a*,*c*) solid line, basal edge Peierls; dotted line, basal screw Peierls; dashed line, prism edge Peierls; dot-dashed line, prism screw Peierls; (*b*,*d*) solid line, basal theoretical strength; dotted line, prism theoretical strength; small-dashed line, pyramidal theoretical strength; double dot-dashed line, rhombohedral theoretical strength; long dashed line, basal twinning; single dot-dashed line, rhombohedral twinning.

For each orientation, during the uniaxial loading process, resolved shear stresses τ for various inelastic deformation modes were computed. For slip, $\tau = \max|\bar{\tau}^i|$, where $i \in$ all basal or prism slip systems; for twinning, $\tau = \max\bar{\tau}^j$, where $j \in$ all basal or rhombohedral twin systems. For fracture, τ is computed as the maximum resolved Kirchhoff stress in any in-plane direction among each of the basal, prism, pyramidal or rhombohedral planes. Pyramidal slip is not considered in this analysis, since experiments are inconclusive regarding its occurrence in the room temperature regime. Pyramidal slip has been observed in *c*-axis sapphire filaments stretched at temperatures in excess of 2000 K, and is thought to be controlled by point defect diffusion and dislocation climb (Tressler & Barber 1974). Selected results are shown in figure 4, with the shear stresses τ normalized by the theoretical estimates τ_C for slip, twinning and fracture of (4.1)–(4.3) and tables 5–7. Volumetric strains corresponding to the HEL (Graham & Brooks 1971; Hare *et al.* 2002) are shown with vertical dotted lines. In the 60°-oriented crystal, as shown in figure 4*a*, prism slip could be activated well before attainment of the HEL, if the Peierls approximation (4.1) is accurate. This agrees with experimental observations of $1/3 < 1\bar{1}00>$ partial dislocations in shock-loaded crystals of the same orientation (Chen & Howitt 1998). Stresses that would

cause twinning or shear fracture are depicted in figure 4*b* for a 60°-oriented crystal. Among the mechanisms shown in figure 4*b*, basal twinning is predicted as most probable, in agreement with the experiments (Chen & Howitt 1998). Regarding fracture, failure on rhombohedral or prism planes is most likely, but theoretical fracture stresses from (4.3) are not attained. Shown in figure 4*c* are shear stresses for glide normalized by the corresponding Peierls barriers (4.1) for a crystal in the rhombohedral (R) orientation. Prism slip seems feasible here at or below the HEL. Stresses for twinning or fracture are shown in figure 4*d*. Basal twinning appears most likely among these mechanisms, and normalized driving forces for shear fracture on pyramidal, prism and basal planes are also significant. Similar analysis of results for the 90° orientation (not shown in figure 4) predicts that for a 90°-oriented crystal, prism slip below the HEL is possible according to the Peierls barrier, twinning is unlikely and pyramidal fracture is the most likely shear failure mechanism. In the 0°-oriented crystal (not shown in figure 4), slip is impossible for the present set of loading conditions. Rhombohedral twinning is most likely, and could occur prior to attainment of the HEL if theoretical estimate (4.2) is accurate. Among potential fracture sites, failure on rhombohedral planes is most likely, but the theoretical limit from (4.3) is never attained. It thus appears likely that nucleated defects such as intersecting twins or dislocation pile-ups could produce stress concentrations enabling fractures in the experiments (Graham & Brooks 1971).

Collectively, the results for different orientations provide the bounds listed in table 8 (in the electronic supplementary material). These bounds are constructed from the assertion that at least one slip or twinning mechanism occurs in a crystal of each considered orientation upon attainment of the volumetric strain corresponding to the experimental HEL for that orientation. The lower bounds suggested in table 8 for fracture on prism, pyramidal and rhombohedral planes ensure that shear fracture would not occur prior to attainment of the experimental HEL in any of the considered crystals. Bounds for fracture on the basal plane are not estimated here. Owing to its relatively high theoretical and cohesive strength (table 7), cleavage fracture on the basal plane seems unlikely. Also shown are bounds relevant for indentation experiments at room temperature (Tymiak & Gerberich 2007). The critical stress for pyramidal slip quoted from Tymiak & Gerberich (2007) is subject to large uncertainty, since it was obtained by extrapolation, and is treated here as a lower bound. The bounds found via consideration of shock physics experiments and nonlinear elasticity are similar to those from indentation (Tymiak & Gerberich 2007), apart from the much higher upper bound listed for basal slip by the latter authors. Confining pressures in indentation were reported of the order of 100 GPa (Tymiak & Gerberich 2007), much higher than those of the order of 10 GPa considered here. Also, plastic strain rates lie in the quasi-static regime in indentation, in contrast to rates in excess of $10^5\,\mathrm{s}^{-1}$ attained in shock-loading experiments (Munson & Lawrence 1979). The similarity in bounds for slip and twinning thus points to rate and pressure independence of initial yield at low to room temperatures. The pressure independence of yield at confining pressures of the order of 1.5 GPa has been confirmed experimentally for prism slip (Castaing *et al.* 1981). However, in shock experiments, plastic strain rates are not constant, but ramp up from small values at the onset of yielding at the front of the plastic wave to values estimated in excess of $10^5\,\mathrm{s}^{-1}$ in the wake of the plastic wavefront (Munson & Lawrence 1979), with

the maximum rate depending on the material and the severity of the impact loading. While significant rate dependence of twinning has not been observed (Scott & Orr 1983), minor rate sensitivities of pyramidal slip with $m \sim 10$ (Tressler & Barber 1974) and prism slip with $m \sim 16$ (Castaing *et al.* 1981) have been observed at low loading rates and very high temperatures. Because strain rates are very large in impact experiments, viscous drag acting on dislocations behind shock fronts (Gilman 1979) could probably elevate the flow stress for slip or twinning such that fracture stresses on prism, pyramidal and rhombohedral planes would be exceeded soon after initial yield, in the wake of the plastic wavefront.

(*c*) *Yield*

The flow stresses $\{\bar{g}\}$ entering (3.45)–(3.47) are expressed as sums of contributions of various mechanisms, e.g. following Kocks *et al.* (1975) or Clayton (2005)

$$\bar{g}^i = g_S^i + g_L^i, \quad \bar{g}_j^i = g_{jS}^i + g_{jL}^i, \quad \bar{g}^j = g_S^j + g_L^j. \tag{4.4}$$

Here, $g_S^i = \bar{g}_{t=0}^i$ reflects the initial yield stress for slip in the parent crystal on system i, and g_L^i reflects long-range barriers associated with defects that accumulate during the deformation history. Analogous definitions apply for resistance to slip within the twins and resistance to twinning in the second and third of (4.4), respectively. Both terms in each sum in (4.4) depend on temperature; the first, i.e. initial yield, is addressed here for sapphire, and the second term is addressed in §4*d*. The initial yield stress depends on short-range interactions such as strong Peierls barriers in crystals with low initial defect densities and non-metallic bonds (Friedel 1964; Farber *et al.* 1993), and at high rates also accounts for viscous, phonon and electron drag (Kocks *et al.* 1975; Gilman 1979). Short-range barriers exhibit a strong temperature dependence for both slip and twinning in sapphire (Lagerlof *et al.* 1994), reflected appropriately by

$$g_S^i = g_0^i \exp(-\lambda^i \theta/\theta_M), \qquad g_S^j = g_0^j \exp(-\lambda^j \theta/\theta_M), \tag{4.5}$$

where g_0^i is an athermal yield stress; θ_M is the melting temperature; and λ^i is a dimensionless parameter. In the second of (4.5), analogous definitions apply for quantities associated with twin system j. Appropriate forms for the temperature dependence of the second of (4.4), i.e. for slip systems within twinned regions, have not been verified experimentally, but it may be reasonable to assume that the short-range barriers for a slip system in the parent are transferred to its rotated counterpart in a twin. Relation (4.5) does not conform to the usual Arrhenius form for thermally activated kinetics (Kocks *et al.* 1975), but can be rationalized in terms of activation volumes for cross-slip in sapphire (Lagerlof *et al.* 1994). Values of g_0 and λ are listed in table 9 (in the electronic supplementary material) for basal, prism and pyramidal slip and basal and rhombohedral twinning. Comparisons with experimental data are given in figure 5. Room temperature experimental values are taken from the first column of results in table 8, except for pyramidal slip whose strength is taken from the rightmost column in table 8 (Tymiak & Gerberich 2007). Pressure and rate dependence are neglected following the discussion in §4*b*, but could be included in a more refined analysis if supporting data become available for all slip and twin system families. High-temperature data for basal and prism slip are

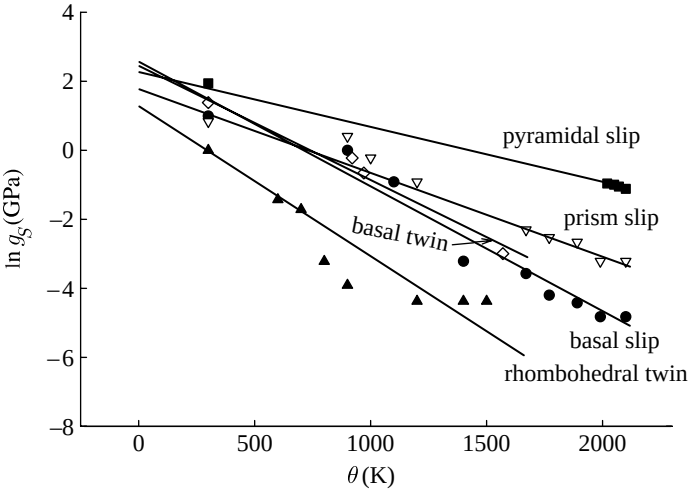

Figure 5. Experimental shear stresses for initial yield by slip or twinning. Circles, basal slip; down triangles, prism slip; squares, pyramidal slip; diamonds, basal twin; up triangles, rhombohedral twin; solid line, model.

obtained from Lagerlof *et al.* (1994). Data for pyramidal slip are obtained from Tressler & Barber (1974). For basal twinning, data are obtained from Castaing *et al.* (2004), and for rhombohedral twinning, from Scott & Orr (1983). For twinning, the fits are most appropriate for $300 \leq \theta \leq 1600$ K, while for slip the model validly spans the range $300 \leq \theta \leq 2100$ K. Trend lines extended down to 0 K are extrapolations. Predictions at 300 K follow

$$g_S^{\text{pyramidal slip}} > g_S^{\text{basal twin}} \approx g_S^{\text{basal slip}} > g_S^{\text{prism slip}} > g_S^{\text{rhombohedral twin}}, \tag{4.6}$$

in general agreement with the trends of table 8. A kink pair-based model (Rodriguez *et al.* 2008) may offer more accuracy for basal and prism slip at high temperatures, albeit with more parameters.

(*d*) *Hardening and lattice defects*

Potentially, the long-range barriers in each of (4.4) could depend in a complex manner upon activity of the slip or twin system under consideration (i.e. self-hardening) as well as the activity of all other slip and twin systems (Christian & Mahajan 1995; Wu *et al.* 2007). Considered here are phenomena for which supporting data are available: hardening of slip and hardening of twinning by dislocation accumulation. To address the former, let

$$\dot{g}_L^i = \left(1 - g_L^i/g_M^i\right) h^i \sum_{k=1}^{n} |\dot{\gamma}^k|, \qquad g_L^i|_{t=0} = 0, \tag{4.7}$$

where g_M^i is a saturation stress (Wu *et al.* 2007) and h^i is a hardening modulus. These vary with the thermodynamic state of the crystal as

$$g_M^i = g_m^i \exp(-\omega^i \theta/\theta_M), \qquad h^i = \mu\left(h_0^i - h_1^i \theta/\theta_M\right), \tag{4.8}$$

where g^i_m, ω^i, h^i_0 and h^i_1 are constants that may differ among families of slip systems. Relations (4.7) and (4.8) provide a reasonable fit to the basal slip data of Pletka *et al.* (1977), with model parameters listed in table 9. Dislocation accumulation takes place in conjunction with slip system hardening via

$$g^i_L = \alpha^i \mu b \sqrt{\rho_{\mathrm{T}} - \rho_{\mathrm{T}0}}, \quad \alpha^i = \alpha^i_0 - \alpha^i_1 \theta/\theta_M, \tag{4.9}$$

where $\rho_{\mathrm{T}0}$ is the initial dislocation density and α^i_0 and α^i_1 are dimensionless constants that may vary among slip systems. Following Pletka *et al.* (1977), (4.9) extends the theory of Taylor (1934) of slip impedance from dislocation interactions on parallel planes. Parameters are listed in table 9 following calibration to data from experiments at a rate of $\dot{\gamma}^P \approx \dot{\gamma}_S = 1.33 \times 10^{-4}\,\mathrm{s}^{-1}$ (Pletka *et al.* 1977), with γ^P the cumulative plastic shear. Relation (4.9) can be inverted and used with (4.7) to provide an evolution equation for the accumulated dislocation line density (Clayton 2005). Note that h^i and g^i_L are scaled consistently by the rhombohedral shear modulus μ that depends on temperature (table 2). Experiments also provide quantitative evidence for the hardening of rhombohedral twin propagation by accumulation of forest dislocations (Castaing *et al.* 2002). Hardening of twinning by slip is captured, in general, by

$$\dot{g}^j_L = \sum_{i=1}^{n} h^j_i \dot{g}^i_L, \quad g^j_L|_{t=0} = 0, \tag{4.10}$$

where h^j_i is an interaction matrix relating the hardening rate of slip system i to that of twin fraction j. Parameter $h^j_i = h_r \delta^j_i$ found from a fit to data of Castaing *et al.* (2002) is given in table 9, applicable only for the hardening of rhombohedral twinning by basal slip. Hardening of prism and pyramidal slip systems and basal twin systems by dislocation accumulation has not yet been addressed. Twin–twin interactions, hardening of slip systems within twins and hardening of slip by twinning also remain to be quantified.

Stored elastic energies of dislocation lines (energy per unit length) and twin boundaries (energy per unit area) are written as

$$\left.\begin{aligned} W_{\mathrm{D}} &= (\mu b^2/(4\pi K))\ln(R/R_C) + \hat{W} \approx \kappa_1 \mu b^2/2, \\ W_{\mathrm{T}} &\approx W_{\mathrm{SF}}/2 = \kappa_2 \mu b/2 \end{aligned}\right\} \tag{4.11}$$

where in the first of (4.11), K accounts for the edge or screw character of the dislocation line as well as elastic anisotropy (Eshelby 1949); R is the radial distance from the dislocation core; R_C is the cut-off radius for the dislocation core; and $\hat{W}$ is a correction that accounts for the core energy, line curvature, interaction energies from other defects and boundaries, and stacking faults associated with partial slip dislocations. As an order-of-magnitude approximation (Hull & Bacon 1984; Heuer *et al.* 1998), here $\kappa_1 = 2.0/K$ is assumed. Elastic anisotropy is neglected in this context, and K follows from (4.1). Recall from §3*d* and table 6 that $W_{\mathrm{SF}} \sim 1-10\ \mathrm{J\,m}^{-2}$ is a typical stacking fault energy associated with twin systems, from which κ_2 entering (3.42) can be quantified as $W_{\mathrm{SF}}/\mu b$.

Consider now the net energy accumulated in the crystal during single slip at constant temperature. From (4.11), and again assuming that rate effects on flow stress are negligible, the cumulative value β of the dissipation fraction β' in (3.44)

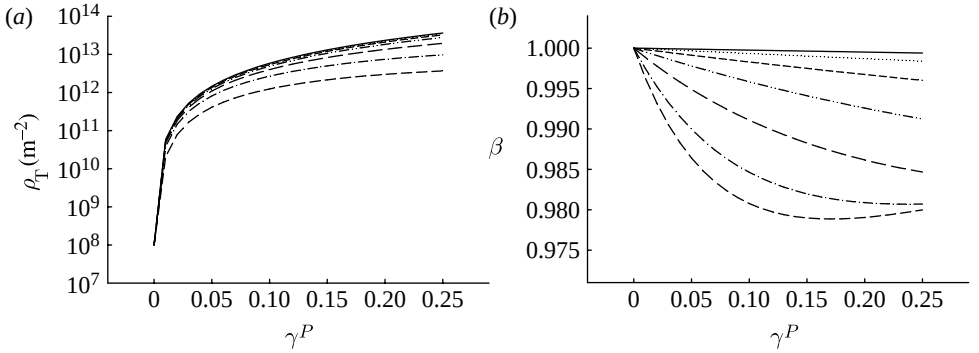

Figure 6. Model predictions for slip on the basal plane: (*a*) dislocation density accumulation and (*b*) cumulative heat dissipation fraction from edge dislocations. (Solid line, 0 K; dotted line, 300 K; small-dashed line, 600 K; double dot-dashed line, 900 K; long-dashed line, 1200 K; single dot-dashed line, 1500 K; medium-dashed line, 1800 K.)

can be approximated as

$$\beta = \left(\int \bar{g}^i \mathrm{d}\gamma^i - \mu b^2 \rho_{\mathrm{T}}/K\right)\left(\int \bar{g}^i \mathrm{d}\gamma^i\right)^{-1} \quad \text{(single slip)}. \tag{4.12}$$

During basal slip, dislocations are predicted, by inversion of (4.9), to accumulate as shown in figure 6*a*. The corresponding dissipation fraction β is shown in figure 6*b*, computed via integration of (4.7) and use of (4.9), (4.12) and material parameters obtained from fits to high-temperature data (Pletka *et al.* 1977). Since during the experiments (Pletka *et al.* 1977) dislocations of families with various strengths and orientations were generated, in the computations, the representative value used for b is the rhombohedral lattice parameter and used for μ is the rhombohedral shear modulus. Shown in figure 6*b* are results for edge dislocations; screw dislocations would result in a decrease in energy storage, $1-\beta$, by a factor of $K=0.76$. Note from figure 6*a* that the dislocation densities increase with plastic shear from the initial value $\rho_{\mathrm{T}0}=10^8\ \mathrm{m}^{-2}$ (Pletka *et al.* 1977) to saturation values in the range $10^{12}\ \mathrm{m}^{-2}$ $\rho_{\mathrm{T}}<10^{14}\ \mathrm{m}^{-2}$ that increase with decreasing temperature. Predicted values of β approach unity as the temperature decreases, primarily a result of the high basal slip resistance of sapphire at low temperatures, which leads to large dissipation from plastic work. At all temperatures, the stored energy appears small relative to the plastic work, since $\beta>0.975$.

(*e*) *Residual volume changes*

The residual volume change $\bar{J}$ was introduced following relations (3.2) and (3.11). An estimate of this quantity from nonlinear elasticity theory is (Seeger & Haasen 1958; Teodosiu 1982)

$$\bar{J} - 1 = \Delta V/V_0 \approx \frac{1}{B}\left(\frac{\partial B}{\partial p} - 1\right)E_{\mathrm{V}} + \frac{1}{G}\left(\frac{\partial G}{\partial p} - \frac{G}{B}\right)E_{\mathrm{S}}, \tag{4.13}$$

where G and B are shear and bulk moduli; p is the Cauchy pressure; and E_{V} and E_{S} are dilatational and deviatoric strain energies per unit volume, respectively. The volume change in (4.13) is measured between reference and intermediate

configurations: $\Delta V = \bar{V} - V_0$ with $\bar{V}$ the volume in $\bar{B}$. Partitioning the elastic energies per unit dislocation line length in the first of (4.11) into dilatational and deviatoric components and neglecting core and interaction energies, (4.13) can be written as (Seeger & Haasen 1958; Teodosiu 1982)

$$\frac{\Delta V}{V_0} \approx \begin{cases} \dfrac{1}{3}\left[\dfrac{1-\nu-2\nu^2}{(1-\nu)B}\left(\dfrac{\partial B}{\partial p}-1\right)+\dfrac{2-2\nu+2\nu^2}{(1-\nu)G}\left(\dfrac{\partial G}{\partial p}-\dfrac{G}{B}\right)\right] W_{\mathrm{D}}\rho_{\mathrm{T}} \quad \text{(edge)}, \\ \dfrac{1}{G}\left(\dfrac{\partial G}{\partial p}-\dfrac{G}{B}\right) W_{\mathrm{D}}\rho_{\mathrm{T}} \quad \text{(screw)}. \end{cases} \tag{4.14}$$

Expressions (4.13) and (4.14) neglect anisotropy. An exact solution for the residual elastic volume change, and possibly shape change, in a highly anisotropic (e.g. rhombohedral) lattice seems to require integration over local elastic displacement gradients induced by defects within the body (Toupin & Rivlin 1960). Closed-form expressions for residual elastic volume change exist for anisotropic single crystals of cubic symmetry (Toupin & Rivlin 1960), and have been applied in analysis of volume changes from stored energy of cold work in metal polycrystals (Wright 1982). Here, following previous work (Seeger & Haasen 1958), isotropic approximation (4.14) is investigated as an order-of-magnitude estimate, consistent with the isotropic approximation of dislocation energies in the first of (4.11). Table 10 (in the electronic supplementary material) lists values of the normalized volume change $\Delta V/(Lb^2)$, where L is the total length of dislocation lines of pure screw or pure edge character, and b is the Burgers vector. For alumina, effective isotropic constants (Holm *et al.* 1999) and their pressure derivatives (Sarkar *et al.* 1996) are obtained from the literature and are valid at room temperature. Values of the normalized volume change in Al_2O_3 from dislocation lines are positive in agreement with other solids (Seeger & Haasen 1958; Wright 1982), and fall in between those for metallic crystal Cu (face-centred cubic) and ionic crystal NaCl (cubic rock salt structure), with properties of the latter two solids given by Seeger & Haasen (1958) also listed in table 10. Experimental data for inelastic volume changes and dislocation densities are available for Cu polycrystals (Clarebrough *et al.* 1957); the range of values for the volume change in the rightmost column of table 10 corresponds to applied compressive strains ranging from 0.3–0.7. Thus, the theory underestimates the volume change by a factor of approximately 2–5 for Cu polycrystals. The linear relationship between the dislocation density and volume change in (4.14) is evident. Wright (1982) noted that the ratio of dilatational to deviatoric stored energy may change during the course of large deformation; this could lead to nonlinearity not captured by either of the estimates in (4.14) alone. Volume changes predicted by (4.14) remain small as saturation levels of dislocation density implied by figure 6*a* are approached. For example, a density of edge dislocations $\rho_{\mathrm{T}} = 10^{14}\,\mathrm{m}^{-2}$ would produce a volume change $\Delta V/V_0 \approx 4\times 10^{-5}$, corresponding to the volume increase that would result from thermal expansion in alumina upon a temperature rise of approximately 2.5 K. However, according to the theory, volume increases of the order of 1 per cent would be achieved upon generation of immense dislocation densities, e.g. $\rho_{\mathrm{T}} \sim 10^{16}\,\mathrm{m}^{-2}$, corresponding to a dislocation spacing of the order of 10 nm. Conceivably, very large dislocation densities may be required to enable extremely large plastic

strain rates in shock physics experiments if the upper bound of the dislocation velocity is limited to that of transverse elastic waves in the crystal (Kocks *et al.* 1975). Generation of defect densities of this magnitude could affect the measured pressure–volume response; for example, the pressure required to offset a 1 per cent volume increase would be of the order of $0.01B=2.5$ GPa. One should keep in mind the limits of the continuum elasticity approximations used in (4.11) and (4.14). Atomistic simulations (Clayton & Chung 2006) may offer the possibility of more accurate predictions of effects of large defect densities on volume changes, effective moduli and stored energies.

5. Conclusions

The theory developed here focuses on anisotropic mechanisms of elasticity, plastic slip and deformation twinning. Large deformation theory is required to address finite shears arising from slip and twinning, lattice reorientations arising from twinning and nonlinear elastic effects. A constitutive framework incorporating internal state variables provides thermodynamic relationships among state variables and driving forces for inelastic deformations. The application represents the first, to the author's knowledge, fully nonlinear anisotropic, crystal plasticity-based model for the ensemble of observed thermoelastic and inelastic behaviours of sapphire. Inelastic behaviours include basal, prism and pyramidal slip and basal and rhombohedral twinning. Estimates of room temperature resistances to slip or twin initiation follow from nonlinear thermoelastic analysis and results of prior shock physics experiments (Barker & Hollenbach 1970; Graham & Brooks 1971; Chen & Howitt 1998; Hare *et al.* 2002; Reinhart *et al.* 2006). These estimates are combined with other existing data to provide yield criteria over a range of temperatures. Hardening from dislocation accumulation during basal slip is quantified, and residual elastic energies associated with defects are estimated. The cumulative ratio of stored energy from dislocations to dissipated energy in basal slip is predicted at less than 3 per cent for plastic shears of less than 0.25. Residual volume expansion from nucleation of dislocation lines is estimated using nonlinear elasticity theory (Seeger & Haasen 1958; Teodosiu 1982). Such expansion is predicted to be nearly negligible in sapphire for dislocation line densities observed in high-temperature experiments (Pletka *et al.* 1977).

References

Asaro, R. J. 1983 Crystal plasticity. *ASME J. Appl. Mech.* **50**, 921–934.

Azdhari, A. & Nemat-Nasser, S. 1998 Experimental and computational study of fracturing in an anisotropic brittle solid. *Mech. Mater.* **28**, 247–262. (doi:10.1016/S0167-6636(97)00062-8)

Barker, L. M. & Hollenbach, R. E. 1970 Shock-wave studies of PMMA, fused silica, and sapphire. *J. Appl. Phys.* **41**, 4208–4226. (doi:10.1063/1.1658439)

Bernstein, N. & Tadmor, E. B. 2004 Tight-binding calculations of stacking energies and twinnability in fcc metals. *Phys. Rev. B* **69**, 094 116. (doi:10.1103/PhysRevB.69.094116)

Bhattacharya, K. 1991 Wedge-like microstructure in martensites. *Acta Metall. Mater.* **39**, 2431–2444. (doi:10.1016/0956-7151(91)90023-T)

Bilby, B. A. & Crocker, A. G. 1965 The theory of the crystallography of deformation twinning. *Proc. R. Soc. A* **288**, 240–255. (doi:10.1098/rspa.1965.0216)

Born, M. & Huang, K. 1954 *Dynamical theory of crystal lattices*. Oxford, UK: Oxford University Press.

Bourne, N. K., Millett, J. C. F., Chen, M., McCauley, J. W. & Dandekar, D. P. 2007 On the Hugoniot elastic limit in polycrystalline alumina. *J. Appl. Phys.* **102**, 073 514. (doi:10.1063/1.2787154)

Brugger, K. 1964 Thermodynamic definition of higher order elastic coefficients. *Phys. Rev.* **133**, A1611–A1612. (doi:10.1103/PhysRev.133.A1611)

Castaing, J., Cadoz, J. & Kirby, S. H. 1981 Prismatic slip of Al_2O_3 single crystals below 1000°C in compression under hydrostatic pressure. *J. Am. Ceram. Soc.* **64**, 504–511. (doi:10.1111/j.1151-2916.1981.tb10314.x)

Castaing, J., Munoz, A. & Dominguez Rodriguez, A. 2002 Hardening of rhombohedral twinning in sapphire (α-Al_2O_3) by basal slip dislocations. *Philos. Mag. A* **82**, 1419–1431.

Castaing, J., He, A., Lagerlof, K. P. D. & Heuer, A. H. 2004 Deformation of sapphire (α-Al_2O_3) by basal slip and basal twinning below 700°C. *Philos. Mag.* **84**, 1113–1125. (doi:10.1080/14786430310001613183)

Chen, S.-J. & Howitt, D. G. 1998 Observations of partial dislocations and basal twin boundaries in shock-wave-deformed sapphire. *Philos. Mag. A* **78**, 765–776. (doi:10.1080/01418619808241935)

Chin, G. Y., Hosford, W. F. & Mendorf, D. R. 1969 Accommodation of constrained deformation in FCC metals by slip and twinning. *Proc. R. Soc. A* **309**, 433–456. (doi:10.1098/rspa.1969.0051)

Christian, J. W. & Mahajan, S. 1995 Deformation twinning. *Prog. Mater. Sci.* **39**, 1–157. (doi:10.1016/0079-6425(94)00007-7)

Clarebrough, L. M., Hargreaves, M. E. & West, G. W. 1957 The density of dislocations in compressed copper. *Acta Metall.* **5**, 738–740. (doi:10.1016/0001-6160(57)90076-7)

Clayton, J. D. 2005 Dynamic plasticity and fracture in high density polycrystals: constitutive modeling and numerical simulation. *J. Mech. Phys. Solids* **53**, 261–301. (doi:10.1016/j.jmps.2004.06.009)

Clayton, J. D. & Chung, P. W. 2006 An atomistic-to-continuum framework for nonlinear crystal mechanics based on asymptotic homogenization. *J. Mech. Phys. Solids* **54**, 1604–1639. (doi:10.1016/j.jmps.2006.02.004)

Clayton, J. D., Bammann, D. J. & McDowell, D. L. 2005 A geometric framework for the kinematics of crystals with defects. *Philos. Mag.* **85**, 3983–4010. (doi:10.1080/14786430500363312)

Coleman, B. D. & Noll, W. 1963 The thermodynamics of elastic materials with heat conduction and viscosity. *Arch. Rat. Mech. Anal.* **13**, 167–178. (doi:10.1007/BF01262690)

Eshelby, J. D. 1949 Edge dislocations in anisotropic materials. *Philos. Mag.* **40**, 903–912.

Eshelby, J. D. 1975 The elastic energy-momentum tensor. *J. Elasticity* **5**, 321–335. (doi:10.1007/BF00126994)

Farber, Y. A., Yoon, S. Y., Lagerlof, K. P. D. & Heuer, A. H. 1993 Microplasticity during high temperature indentation and the Peierls potential of sapphire (α-Al_2O_3) single crystals. *Phys. Stat. Solidi A* **137**, 485–498. (doi:10.1002/pssa.2211370219)

Frenkel, J. 1926 Zur theorie der elastizitatsgrenze und der festigkeit kristallinischer korper. *Z. Phys.* **37**, 572–609. (doi:10.1007/BF01397292)

Friedel, J. 1964 *Dislocations*. Oxford, UK: Pergamon.

Gilman, J. J. 1979 Resistance to shock-front propagation in solids. *J. Appl. Phys.* **50**, 4059–4064. (doi:10.1063/1.326487)

Graham, R. A. & Brooks, W. P. 1971 Shock-wave compression of sapphire from 15 to 420 kbar. The effects of large anisotropic compressions. *J. Chem. Phys. Solids* **32**, 2311–2330. (doi:10.1016/S0022-3697(71)80226-3)

Hare, D. E., Holmes, N. C. & Webb, D. J. 2002 Shock-wave-induced optical emission from sapphire in the stress range 12 to 45 GPa: images and spectra. *Phys. Rev. B* **66**, 014 108. (doi:10.1103/PhysRevB.66.014108)

Heuer, A. H., Lagerlof, K. P. D. & Castaing, J. 1998 Slip and twinning dislocations in sapphire (α-Al_2O_3). *Philos. Mag. A* **78**, 747–763. (doi:10.1080/01418619808241934)

Hirth, J. P. & Lothe, J. 1982 *Theory of dislocations*. New York, NY: Wiley.

Holm, B., Ahuja, R., Yourdshahyan, Y., Johansson, B. & Lundqvist, B. I. 1999 Elastic and optical properties of α- and κ-Al_2O_3. *Phys. Rev. B* **59**, 12 777–12 787. (doi:10.1103/PhysRevB.59.12777)

Hull, D. & Bacon, D. J. 1984 *Introduction to dislocations*, 3rd edn. Oxford, UK: Butterworth-Heinemann.

Hutchinson, J. W. 1976 Bounds and self-consistent estimates for creep of polycrystalline materials. *Proc. R. Soc. A* **348**, 101–127. (doi:10.1098/rspa.1976.0027)

Kalidindi, S. R. 1998 Incorporation of deformation twinning in crystal plasticity models. *J. Mech. Phys. Solids* **46**, 267–290. (doi:10.1016/S0022-5096(97)00051-3)

Klassen-Neklyudova, M. V., Govorkov, V. G., Urusovskaya, A. A., Voinova, N. N. & Kozlovskaya, E. P. 1970 Plastic deformation of corundum single crystals. *Phys. Stat. Solidi* **39**, 679–688. (doi:10.1002/pssb.19700390236)

Kocks, U. F., Argon, A. S. & Ashby, M. F. 1975 Thermodynamics and kinetics of slip. *Prog. Mater. Sci.* **19**, 1–288. (doi:10.1016/0079-6425(75)90005-5)

Kronberg, M. L. 1957 Plastic deformation of single crystals of sapphire: basal slip and twinning. *Acta Metall.* **5**, 507–524. (doi:10.1016/0001-6160(57)90090-1)

Lagerlof, K. P. D., Heuer, A. H., Castaing, J., Riviere, J. P. & Mitchell, T. E. 1994 Slip and twinning in sapphire (α-Al_2O_3). *J. Am. Ceram. Soc.* **77**, 385–397. (doi:10.1111/j.1151-2916.1994.tb07006.x)

Lankford, J., Predebon, W. W., Staehler, J., Subhash, G., Pletka, B. & Anderson, C. 1998 The role of plasticity as a limiting factor in the compressive failure of high strength ceramics. *Mech. Mater.* **29**, 205–218. (doi:10.1016/S0167-6636(98)00023-4)

Munson, D. E. & Lawrence, R. J. 1979 Dynamic deformation of polycrystalline alumina. *J. Appl. Phys.* **50**, 6272–6282. (doi:10.1063/1.325766)

Peierls, R. E. 1940 The size of a dislocation. *Proc. Phys. Soc.* **52**, 34–37. (doi:10.1088/0959-5309/52/1/305)

Pletka, B. J., Heuer, A. H. & Mitchell, T. E. 1977 Work-hardening in sapphire (α-Al_2O_3). *Acta Metall.* **25**, 25–33. (doi:10.1016/0001-6160(77)90242-5)

Reinhart, W. D., Chhabildas, L. C. & Vogler, T. J. 2006 Investigating the phase transitions and strength in single-crystal sapphire using shock–reshock loading techniques. *Int. J. Impact Eng.* **33**, 655–669. (doi:10.1016/j.ijimpeng.2006.09.083)

Rodriguez, M. C., Castaing, J., Munoz, A., Veyssiere, P. & Rodriguez, A. D. 2008 Analysis of a kink pair model applied to a Peierls mechanism in basal and prism plane slips in sapphire (α-Al_2O_3) deformed between 200° and 1800°C. *J. Am. Ceram. Soc.* **91**, 1612–1617. (doi:10.1111/j.1551-2916.2008.02317.x)

Sarkar, S., Ballabh, T. K., Middya, T. R. & Basu, A. N. 1996 *T*-matrix approach to effective nonlinear elastic constants of heterogeneous materials. *Phys. Rev. B* **54**, 3926–3931. (doi:10.1103/PhysRevB.54.3926)

Scott, W. D. & Orr, K. K. 1983 Rhombohedral twinning in alumina. *J. Am. Ceram. Soc.* **66**, 27–32. (doi:10.1111/j.1151-2916.1983.tb09962.x)

Seeger, A. & Haasen, P. 1958 Density changes of crystals containing dislocations. *Philos. Mag.* **3**, 470–475.

Snow, J. D. & Heuer, A. H. 1973 Slip systems in Al_2O_3. *J. Am. Ceram. Soc.* **56**, 153–157. (doi:10.1111/j.1151-2916.1973.tb15432.x)

Taylor, G. I. 1934 The mechanism of plastic deformation of crystals. *Proc. R. Soc. A* **145**, 362–415. (doi:10.1098/rspa.1934.0106)

Taylor, G. I. & Quinney, H. 1934 The latent energy remaining in a metal after cold working. *Proc. R. Soc. A* **143**, 307–326. (doi:10.1098/rspa.1934.0004)

Teodosiu, C. 1982 *Elastic models of crystal defects*. Berlin, Germany: Springer.

Toupin, R. A. & Rivlin, R. S. 1960 Dimensional changes in crystals caused by dislocations. *J. Math. Phys.* **1**, 8–15. (doi:10.1063/1.1703638)

Tressler, R. E. & Barber, D. J. 1974 Yielding and flow of *c*-axis sapphire filaments. *J. Am. Ceram. Soc.* **57**, 13–19. (doi:10.1111/j.1151-2916.1974.tb11353.x)

Tymiak, N. I. & Gerberich, W. W. 2007 Initial stages of contact-induced plasticity in sapphire. I. Surface traces of slip and twinning. *Philos. Mag.* **87**, 5143–5168. (doi:10.1080/14786430701618464)

Van Houtte, P. 1978 Simulation of the rolling and shear texture of brass by the Taylor theory adapted for mechanical twinning. *Acta Metall.* **26**, 591–604. (doi:10.1016/0001-6160(78)90111-6)

Wiederhorn, S. M. 1969 Fracture of sapphire. *J. Am. Ceram. Soc.* **52**, 485–491. (doi:10.1111/j.1151-2916.1969.tb09199.x)

Winey, J. M., Gupta, Y. M. & Hare, D. E. 2001 *R*-axis sound speed and elastic properties of sapphire single crystals. *J. Appl. Phys.* **90**, 3109–3111. (doi:10.1063/1.1391420)

Wright, T. W. 1982 Stored energy and plastic volume change. *Mech. Mater.* **1**, 185–187. (doi:10.1016/0167-6636(82)90011-4)

Wu, X., Kalidindi, S. R., Necker, C. & Salem, A. A. 2007 Prediction of crystallographic texture evolution and anisotropic stress–strain curves during large plastic strains in high purity α-titanium using a Taylor-type crystal plasticity model. *Acta Mater.* **55**, 423–432. (doi:10.1016/j.actamat.2006.08.034)

Zhang, C., Kalia, R. K., Nakano, A. & Vashishta, P. 2007 Hypervelocity impact induced deformation modes in α-alumina. *Appl. Phys. Lett.* **91**, 071 906. (doi:10.1063/1.2753092)

Table 1 Room temperature elastic moduli

Parameter	Value [GPa] [1]	Parameter	Value [GPa] [1]	Parameter	Value [GPa] [1]
C_{11}	498	C_{111}	-3780	C_{134}	131
C_{12}	163	C_{112}	-1090	C_{144}	-302
C_{13}	117	C_{113}	-963	C_{155}	-1160
C_{14}	23	C_{114}	-55	C_{222}	-4520
C_{33}	502	C_{123}	-289	C_{333}	-3340
C_{44}	147	C_{124}	39	C_{344}	-1090
		C_{133}	-922	C_{444}	19

[1]Winey et al. [2001]

Table 2 Bulk physical properties (atmospheric pressure)

Parameter	Value	Remarks
ρ_0	3980 kg/m^3	room temperature mass density [1]
c	780+0.3(θ-300) J/kgK	specific heat per unit mass [2]
$\bar{\alpha}_{11}$	5.0×10^{-6} /K	thermal expansion coefficient [1]
$\bar{\alpha}_{33}$	5.7×10^{-6} /K	thermal expansion coefficient [1]
θ_M	2325 K	melting temperature [2]
μ	156-70θ/θ_M GPa	rhombohedral shear modulus [3]

[1]Burghartz & Schultz [1994] [2]Castanet [1984] [3]Zouboulis & Grimsditch [1991]

Table 3 Slip systems

Type	Direction	Plane	Remarks	Type	Direction	Plane	Remarks
basal	$[11\bar{2}0]$	(0001)	bidirectional [1]	pyramidal	$[\bar{1}101]$	$(10\bar{1}1)$	unidirectional [2]
	$[\bar{1}2\bar{1}0]$	(0001)			$[0\bar{1}11]$	$(10\bar{1}1)$	
	$[\bar{2}110]$	(0001)			$[10\bar{1}1]$	$(0\bar{1}11)$	
prism	$[1\bar{1}00]$	$(11\bar{2}0)$	bidirectional [1]		$[\bar{1}101]$	$(0\bar{1}11)$	
	$[10\bar{1}0]$	$(\bar{1}2\bar{1}0)$			$[0\bar{1}11]$	$(\bar{1}101)$	
	$[01\bar{1}0]$	$(\bar{2}110)$			$[10\bar{1}1]$	$(\bar{1}101)$	

[1]Kronberg [1957]; Snow & Heuer [1973]; Heuer et al. [1998] [2]Tressler & Barber [1974]

Table 4 Twin systems

Type	Direction	Plane	Shear	Remarks
basal	$[\bar{1}010]$	(0001)	0.635	type II [1]
	$[1\bar{1}00]$	(0001)		
	$[01\bar{1}0]$	(0001)		
rhombohedral	$[\bar{1}01\bar{1}]$	$(\bar{1}012)$	0.202	type I [2]
	$[01\bar{1}\bar{1}]$	$(01\bar{1}2)$		
	$[1\bar{1}0\bar{1}]$	$(1\bar{1}02)$		

[1]Veit [1921]; Kronberg [1957] [2]Heuer [1966]

Table 5 Slip dislocations and Peierls stresses

Plane	Burgers vector [1]	b [nm]	Peierls, edge [GPa]	Peierls, screw [GPa]
basal	$1/3[11\bar{2}0]$	0.475	9.0	16.9
prism	$1/3[1\bar{1}00]$	0.274	0.3	1.3
pyramidal	$1/3[\bar{1}101]$	0.512	0.7	2.4

[1]Kronberg [1957]; Tressler & Barber [1974]; Lagerlof et al. [1994]

Table 6 Twinning partials, energies, and theoretical nucleation stresses

Plane	Burgers vector [1]	b [nm]	Stacking fault energy [J/m^2] [2]	Nucleation stress [GPa]
basal	$1/3[\bar{1}010]$	0.274	9.0	7.3
rhombohedral	$1/21.9[1\bar{1}0\bar{1}]$	0.071	0.7	3.6

[1]Kronberg [1957]; Geipel et al. [1994]; Heuer et al. [1998] [2]Lagerlof et al. [1984]; Kenway [1993]

Table 7 Planar properties

Plane	Full Burgers vector [nm] [1]	Spacing [nm] [2]	Theoretical shear strength [GPa]	Cohesive energy [J/m^2] [3]
basal $\{0001\}$	0.475	0.216	51.5	>40
prism $\{10\bar{1}0\}$	0.475	0.274	40.5	7.3
pyramidal $\{10\bar{1}1\}$	0.512	0.392	30.6	--
rhombohedral $\{\bar{1}012\}$	0.512	0.348	34.4	6.0

[1]Snow & Heuer [1973] [2]Geipel et al. [1994]; Lagerlof et al. [1994] [3]Wiederhorn [1969]

Table 8 Estimated bounds on shear strengths for slip, twinning, and fracture

Mechanism	τ_C [GPa] present work	τ_C [GPa] indentation [1]
basal slip	$2.7 < \tau_C < 5.0$	$4.8 < \tau_C < 23.7$
prism slip	$2.3 < \tau_C < 5.7$	$2.5 < \tau_C < 4.1$
pyramidal slip	--	$\tau_C > 7.0$
basal twin	$\tau_C > 4.0$	$4.8 < \tau_C < 7.3$
rhombohedral twin	$1.0 < \tau_C < 8.1$	$1.0 < \tau_C < 7.3$
prism fracture	$\tau_C > 5.9$	--
pyramidal fracture	$\tau_C > 6.7$	--
rhombohedral fracture	$\tau_C > 7.9$	--

[1]Tymiak & Gerberich [2007]

Table 9 Slip and twinning parameters

Parameter	Value	Remarks	Parameter	Value	Remarks
g_0 [GPa]	12.7	basal slip	g_m [GPa]	53.6	basal slip
	6.6	prism slip	ω	10.7	basal slip
	10.0	pyramidal slip	h_0	8.0×10^{-3}	basal slip
	11.5	basal twin	h_1	9.3×10^{-3}	basal slip
	3.4	rhombohedral twin	α_0	0.65	basal slip
λ	8.4	basal slip	α_1	0.70	basal slip
	5.6	prism slip	h_r	0.42	rhombohedral twin
	3.7	pyramidal slip			
	7.7	basal twin			
	10.2	rhombohedral twin			

Table 10 Effective isotropic elastic properties and volume changes associated with dislocations

Crystal	G [GPa]	B [GPa]	ν	$\partial G/\partial p$	$\partial B/\partial p$	$\Delta V/(Lb^2)$ edge	$\Delta V/(Lb^2)$ screw	$\Delta V/(Lb^2)$ experiment [3]
Al_2O_3 [1]	157	250	0.24	1.7	4.2	1.7	1.0	--
NaCl [2]	15	23	0.24	2.0	5.8	2.5	1.4	--
Cu [2]	47	152	0.36	0.8	4.4	1.0	0.5	1.9-2.6 (edge)

[1]Sarkar et al. [1996]; Holm et al. [1999] [2]Seeger & Haasen [1958] [3]Clarebrough et al. [1957]

Supplementary references

Burghartz, S. & Schulz, B. 1994 Thermophysical properties of sapphire, AlN, and $MgAl_2O_4$ down to 70K. *J. Nucl. Mater.* **212**, 1065-1068. (doi:10.1016/0022-3115(94)90996-2)

Castanet, R. 1984 Selected data on the thermodynamic properties of α-alumina. *High Temp. High Press.* **16**, 449-457.

Geipel, T., Lagerlof, K. P. D., Pirouz, P. & Heuer, A. H. 1994 A zonal dislocation mechanism for rhombohedral twinning in sapphire (α-Al_2O_3). *Acta Metall. Mater.* **42**, 1367-1372. (doi:10.1016/0956-7151(94)90154-6)

Heuer, A. H. 1966 Deformation twinning in corundum. *Phil. Mag.* **13**, 379-393. (doi:10.1080/14786436608212616)

Kenway, P. R. 1993 Calculated stacking fault energies in α-Al_2O_3. *Phil. Mag. B* **68**, 171-183. (doi:10.1080/01418639308226398)

Lagerlof, K. P. D., Mitchell, T. E., Heuer, A. H., Riviere, J. P., Cadoz, J., Castaing, J. & Phillips, D. S. 1984 Stacking fault energy in sapphire (α-Al_2O_3). *Acta Metall.* **32**, 97-105. (doi:10.1016/0001-6160(84)90206-2)

Veit, K. 1921 Artificial deformations and transpositions in minerals. *Neues Jahrb. Miner.* **45**, 121-148.

Zouboulis, E. S. & Grimsditch, M. 1991 Refractive index and elastic properties of single-crystal corundum (α-Al_2O_3) up to 2100K. *J. Appl. Phys.* **70**, 772-776. (doi:10.1063/1.349633)

NO. OF COPIES	ORGANIZATION
1 (PDF only)	DEFENSE TECHNICAL INFORMATION CTR DTIC OCA 8725 JOHN J KINGMAN RD STE 0944 FORT BELVOIR VA 22060-6218
1	DIRECTOR US ARMY RESEARCH LAB IMNE ALC HR 2800 POWDER MILL RD ADELPHI MD 20783-1197
1	DIRECTOR US ARMY RESEARCH LAB AMSRD ARL CI OK TL 2800 POWDER MILL RD ADELPHI MD 20783-1197
1	DIRECTOR US ARMY RESEARCH LAB AMSRD ARL CI OK PE 2800 POWDER MILL RD ADELPHI MD 20783-1197

ABERDEEN PROVING GROUND

1	DIR USARL AMSRD ARL CI OK TP (BLDG 4600)

NO. OF
COPIES ORGANIZATION

1 DIRECTOR
US ARMY RESEARCH LAB
AMSRD ARL CI
R NAMBURU
2800 POWDER MILL RD
ADELPHI MD 20783-1197

ABERDEEN PROVING GROUND

48 DIR USARL
AMSRD ARL CI HC
P CHUNG
D GROVE
J KNAP
AMSRD ARL WM
S KARNA
J MCCAULEY
T WRIGHT
AMSRD ARL WM BD
B FORCH
AMSRD ARL WM MA
W NOTHWANG
AMSRD ARL WM MD
B CHEESEMAN
G GAZONAS
AMSRD ARL WM TA
R DONEY
T JONES
S SCHOENFELD
AMSRD ARL WM TC
T BJERKE
T FARRAND
M FERMEN-COKER
L MAGNESS
S SEGLETES
B SCHUSTER
A TANK
W WALTERS
AMSRD ARL WM TD
S BILYK
D CASEM
J CLAYTON (15 CPS)
D DANDEKAR
N GNIAZDOWSKI
M GREENFIELD
Y HUANG
R KRAFT
B LOVE
M RAFTENBERG
E RAPACKI
M SCHEIDLER
T WEERASOORIYA

INTENTIONALLY LEFT BLANK.